# ADVANCING SCIENCE AND SERVICES DURING THE 2015/16 EL NIÑO

## The NOAA El Niño Rapid Response Field Campaign

Randall M. Dole, J. Ryan Spackman, Matthew Newman, Gilbert P. Compo, Catherine A. Smith, Leslie M. Hartten, Joseph J. Barsugli, Robert S. Webb, Martin P. Hoerling, Robert Cifelli, Klaus Wolter, Christopher D. Barnet, Maria Gehne, Ronald Gelaro, George N. Kiladis, Scott Abbott, Elena Akish, John Albers, John M. Brown, Christopher J. Cox, Lisa Darby, Gijs de Boer, Barbara DeLuisi, Juliana Dias, Jason Dunion, Jon Eischeid, Christopher Fairall, Antonia Gambacorta, Brian K. Gorton, Andrew Hoell, Janet Intrieri, Darren Jackson, Paul E. Johnston, Richard Lataitis, Kelly M. Mahoney, Katherine McCaffrey, H. Alex McColl, Michael J. Mueller, Donald Murray, Paul J. Neiman, William Otto, Ola Persson, Xiao-Wei Quan, Imtiaz Rangwala, Andrea J. Ray, David Reynolds, Emily Riley Dellaripa, Karen Rosenlof, Naoko Sakaeda, Prashant D. Sardeshmukh, Laura C. Slivinski, Lesley Smith, Amy Solomon, Dustin Swales, Stefan Tulich, Allen White, Gary Wick, Matthew G. Winterkorn, Daniel E. Wolfe, and Robert Zamora

Acting on climate forecasts in summer 2015, NOAA rapidly designed and executed the first field campaign to intensively observe atmospheric conditions over the tropical Pacific during a strong El Niño.

El Niño–Southern Oscillation (ENSO), a coupled atmosphere–ocean phenomenon originating in the tropical Pacific, has far-reaching impacts on weather, climate, and society (Ropelewski and Halpert 1987; Kiladis and Diaz 1989; Halpert and Ropelewski 1992; McPhaden et al. 2006). The development and provision of skillful ENSO forecasts to the public are central achievements of climate science. These forecasts, informed by increasing understanding of the impacts of tropical oceans on global weather and climate (Trenberth et al. 1998; Barsugli and Sardeshmukh 2002; Scaife et al. 2014), provide early warning of altered risks for high-impact weather and climate events several months to seasons ahead (Glantz 2000). Yet despite its global importance, an ENSO event has never been the specific focus of an atmospheric field campaign. That changed with the strong El Niño of 2015/16, when the National Oceanic and Atmospheric Administration (NOAA; see Table 1 for list of NOAA acronyms) designed and implemented a complex, multiplatform, multiorganizational field campaign to obtain intensive observations during El Niño, from the initial atmospheric response over the tropical Pacific to weather impacts on the U.S. West Coast (Fig. 1).

From spring through early summer 2015, El Niño gathered strength over the tropical Pacific, becoming the second strongest on record by June 2015 (McPhaden 2015), and forecasters became increasingly

confident of a major event (L'Heureux et al. 2017). In July 2015, the NOAA/NWS/CPC and the International Research Institute for Climate and Society (IRI) forecast a more than 90% chance that El Niño would continue through winter 2015/16 and an 80% chance that El Niño would persist into the following spring (CPC/IRI 2015), seasons when U.S. impacts are usually greatest (Kumar and Hoerling 1998). Many ENSO models predicted a strong El Niño with sea surface temperature (SST) anomalies exceeding 2°C for at least three months in a standard El Niño monitoring region (Fig. 2), rivaling the "super" El Niño events of 1982/83 and 1997/98 (L'Heureux et al. 2017).

This early warning presented an exceptional opportunity to advance understanding and predictions of a strong and potentially extreme climate event and its impacts *while the event was ongoing*. Seizing this opportunity, NOAA initiated the El Niño Rapid Response (ENRR). The ENRR included an observational field campaign led by NOAA/ESRL/PSD, together with model experiments intended to optimize the campaign's field strategy and support services during the event. Ultimately, the full ENRR involved coordination across NOAA and important contributions from external partners. Our focus here is on the ENRR field campaign, the first of its kind to intensively observe atmospheric conditions in the region of enhanced deep convection over the central tropical Pacific during an El Niño.

*Drivers and objectives*. The ultimate driver for the ENRR was the potential for El Niño–related impacts. Given the El Niño forecasts, a specific concern was the increased risk for very heavy rainfall in California during winter 2015 into spring 2016, as observed in prior strong El Niño events of 1982/83 and 1997/98. This relationship was reinforced by other observational evidence (Schonher and Nicholson 1989), and consistent with modeling studies suggesting that strong El Niño conditions increase the likelihood for heavy precipitation in California during the cold season (e.g., Kumar and Hoerling 1997; Hoerling and Kumar 2002; Hoell et al. 2016; Kumar and Chen 2017). An ongoing multiyear extreme drought and associated fire damage and vegetation losses in many parts of the state heightened risks of damaging floods and debris flows should heavy rains occur.

The ENRR field campaign itself was additionally motivated by a crucial and time-sensitive consideration. While much research can be conducted after an El Niño, enhanced observations must be made during the event to support real-time operational predictions and monitoring, as well as to obtain data for future research. The ENRR therefore placed a high priority on obtaining additional observations during the event, with a focus on atmospheric conditions near the heart of El Niño over the central tropical Pacific. This region had never been intensively sampled during El Niño. The absence of intensive observations partly reflects the daunting challenges of developing a field campaign within the 3–6-month lead time provided by ENSO forecasts, much less time than is usually required for such efforts (Schiermeier 2015), compounded by logistical complexities of mounting a campaign in the remote part of the tropical Pacific where El Niño is centered.

*ENRR goal and field campaign objectives*. The overarching ENRR goal was to determine the tropical

**AFFILIATIONS:** Dole, Newman, Compo, C. A. Smith, Hartten, Barsugli, Wolter, Gehne, Albers, Cox, de Boer, Dias, Eischeid, Jackson, Johnston, McCaffrey, Mueller, Murray, Persson, Quan, Rangwala, Reynolds, Sakaeda, Sardeshmukh, Slivinski, L. Smith, Solomon, Swales, Tulich, and Wolfe—CIRES, and NOAA/ESRL/Physical Sciences Division, Boulder, Colorado; Spackman*—NOAA/ESRL/Physical Sciences Division, and Science and Technology Corporation, Boulder, Colorado; Webb, Hoerling, Cifelli, Kiladis, Abbott, Darby, DeLuisi, Fairall, Gorton, Hoell, Intrieri, Lataitis, Mahoney, Neiman, Otto, Ray, White, Wick, and Zamora—NOAA/ESRL/Physical Sciences Division, Boulder, Colorado; Barnet and Gambacorta—Science and Technology Corporation, Columbia, Maryland; Gelaro—NASA Goddard Space Flight Center, Greenbelt, Maryland; Akish—Science and Technology Corporation, and NOAA/ESRL/Physical Sciences Division, Boulder, Colorado; Brown—NOAA/ESRL/Global Systems Division, Boulder, Colorado; Dunion—Cooperative Institute for Marine and Atmospheric Studies, University of Miami, and NOAA/Atlantic Oceanographic and Meteorological Laboratory, Miami, Florida; McColl—CIRES, Boulder, Colorado; Dellaripa—Department of Atmospheric Science, Colorado State University, Fort Collins, Colorado; Rosenlof—NOAA/ESRL/Chemical Sciences Division, Boulder, Colorado; Winterkorn—NOAA/NVision Solutions, Diamond, and NOAA National Data Buoy Center, Stennis Space Center, Mississippi
* **CURRENT AFFILIATION:** NASA Ames Research Center, Moffett Field, California
**CORRESPONDING AUTHOR:** Randy Dole, randy.dole@noaa.gov

*The abstract for this article can be found in this issue, following the table of contents.*

DOI:10.1175/BAMS-D-16-0219.1

A supplement to this article is available online (10.1175/BAMS-D-16-0219.2)

In final form 13 October 2017

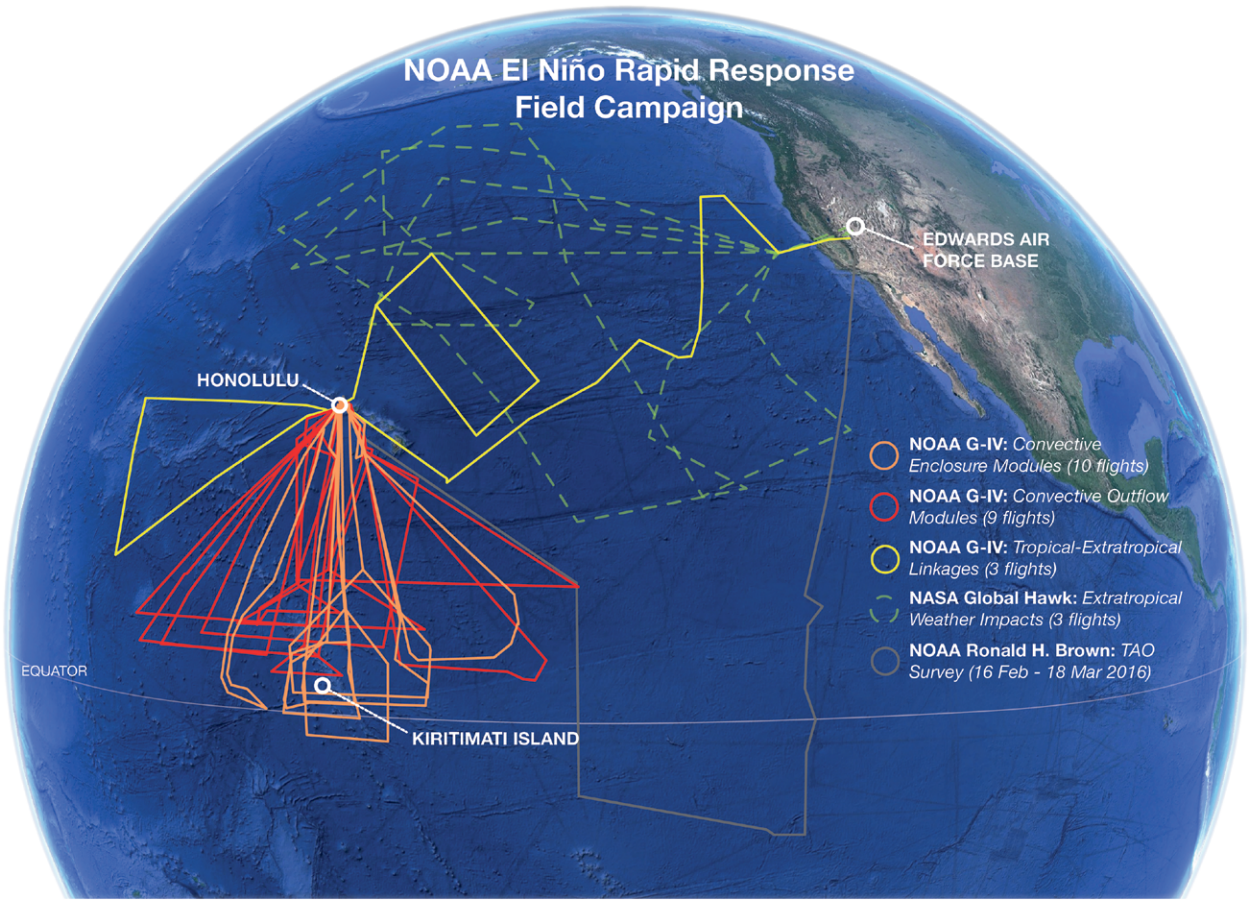


**Fig. 1. Overview of ENRR field campaign coverage by observational platform. Deep tropics convective enclosure flights with the NOAA G-IV (orange tracks), G-IV tropical convective outflow flights (red tracks), G-IV tropical–extratropical linkages flights (yellow tracks), NASA GH flights (dashed green tracks), and *RHB* (silver track). Locations (white circles) of Honolulu and Kiritimati in the Pacific and Edwards Air Force Base in California, the latter being the center for NASA GH operations, are shown. Further details are provided in the text.**

atmospheric response to El Niño and the implications for predicting extratropical storms and U.S. West Coast rainfall. While certain climate anomalies are most common during El Niño, considerable variability occurs from event to event, especially in the extratropics, presenting outstanding science challenges (Capotondi et al. 2015; Deser et al. 2017). In contrast to earlier extratropically focused campaigns (see "Observational field campaigns during prior El Niño events"), the ENRR campaign focused on atmospheric observations over the central tropical Pacific near the largest El Niño–related SST anomalies. It is over this region where El Niño effects on convection and associated divergent outflow were expected to be strongest (Horel and Wallace 1981; Trenberth et al. 1998). The initial atmospheric response to the anomalously warm SSTs serves as a critical first link connecting El Niño to impacts over the United States and around the globe (Fig. 3). The eastward shift of tropical convection following the warmest water leads to an eastward extension and intensification of the Pacific jet, which together with transient variability in tropical convection can alter the frequency, intensity, and paths of extratropical storms impacting the United States and elsewhere.

The ENRR scientific focus is related to a grand challenge in weather and climate models to properly represent tropical convection and its organized dynamical response (e.g., Moncrieff et al. 2012), to which extratropical forecasts can be sensitive (e.g., Barsugli and Sardeshmukh 2002; Bauer et al. 2015). Convective variations in this region would be expected to affect U.S. forecasts on time scales of several days and longer, beyond the lead times considered in earlier extratropical field campaigns (see "Observational field campaigns during prior El Niño events"). As forecast system errors in the El Niño region can reduce skill in medium- and longer-range forecasts over the United States, identifying deficiencies in observational coverage, data assimilation, and model representations of physical processes were overarching

## OBSERVATIONAL FIELD CAMPAIGNS DURING PRIOR EL NIÑO EVENTS

Although not focused over the central tropical Pacific, enhanced field observations have been obtained during prior El Niño events, usually simply by chance. Even when serendipitous, the additional observations have contributed to major scientific advances. During the International Geophysical Year (IGY) of 1957–58, increased ocean and atmospheric observations were obtained during a strong El Niño. The strength of that event together with enhanced IGY observations helped Jacob Bjerknes to achieve fundamental new insights into El Niño as a basinwide atmosphere–ocean phenomenon, with large influences on weather and climate extending well beyond the tropical Pacific into higher latitudes (Bjerknes 1966, 1969). Subsequently, the first forecast for El Niño development was published (Quinn 1974). In response, Klaus Wyrtki proposed an ocean expedition over the far eastern Pacific, with cruises conducted in February–May 1975. Although El Niño failed to develop, the additional observations contributed important insights on tropical ocean dynamics (McPhaden et al. 2015).

More recently, two atmospheric field campaigns were conducted over the eastern extratropical North Pacific during the strong El Niño of 1997/98. The first, the North Pacific Experiment (NORPEX-98), performed aircraft observations over the extratropical North Pacific between the Hawaiian Islands and Alaska from 14 January to 27 February 1998. The primary aim of NORPEX-98 was to apply targeted observations to improve short-range (~2 days) forecasts of landfalling Pacific winter storms on the North American coast (Langland et al. 1999; Shapiro et al. 2001). The second, the California Land-Falling Jets Experiment (CALJET), conducted 26 flights between 18 January and 24 March 1998 over the near offshore and California coast to better understand the effects of a coastal low-level jet, orographic interactions, and microphysical processes on California rainfall (Neiman et al. 2002; Ralph et al. 2003; White et al. 2003). In addition to leading the 1998 field campaigns, throughout this event NOAA, and especially the NWS, together with other organizations proactively communicated risks for potential weather and climate impacts related to the strong El Niño, including heavy precipitation and coastal storms in California (Leetmaa 1999; Chagnon 2000).

science objectives. Science questions and hypotheses for the broader NOAA ENRR, which included model experiments in addition to the field campaign, as well as the specific objectives for the field campaign are provided in Table 2.

**IMPLEMENTATION PLANNING AND COORDINATION.** Perhaps the most basic question in planning the ENRR field campaign was: *Given the narrow time window provided by El Niño forecasts, was a field campaign even possible while the event was ongoing?* Because El Niño forecast lead times are shorter than NOAA's normal planning processes, no prior resources had been allocated for an ENRR field campaign. As a first step, in late summer 2015 PSD redirected previously allocated NOAA Gulfstream-IV (G-IV) flight hours to El Niño–related research and initiated intensive planning to make best use of this resource. Since this flight time would allow only relatively limited observations, a further challenge was to identify and obtain additional necessary assets to conduct a broader field campaign within existing resource allocations. Toward this end, in September 2015 NOAA leadership created an intra-agency ENRR coordination team with representatives from all of NOAA's line offices (Table 1), who reviewed proposed ENRR actions to develop a cohesive intra-agency

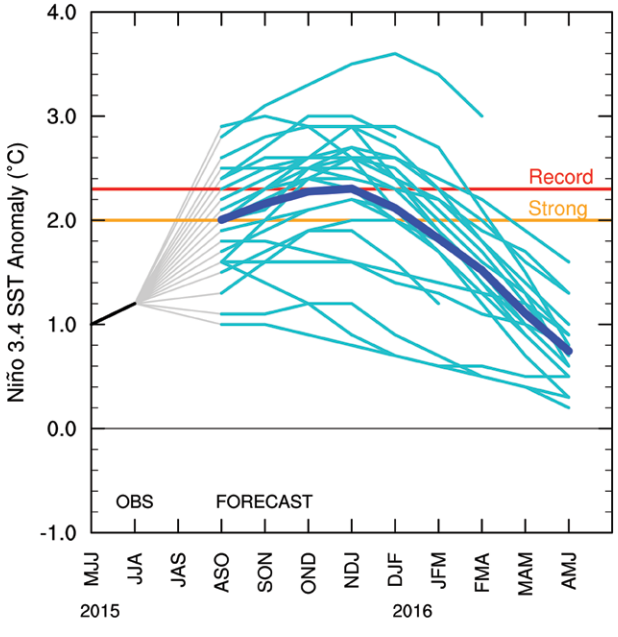


**Fig. 2. Dynamical and statistical model predictions of average Niño-3.4 SST anomalies (°C) initialized in Aug 2015 for running 3-month periods from Aug–Oct (ASO) 2015 to Apr–Jun (AMJ) 2016. Niño-3.4 SST index over the region (5°N–5°S, 170°–120°W) is a commonly used measure in El Niño monitoring and predictions, including impacts over North America. Many individual models (light blue lines) show strong (>2°C) or even record-breaking values during Northern Hemisphere cold season, with the model average (thick blue line) showing near-record values. Since 1950, five El Niño events peaked between 1.5° and 2.0°C, with only two exceeding 2.0°C: 1997/98 (2.3°C) and 1982/83 (2.1°C). Prediction data were obtained from the IRI website (IRI 2017).**

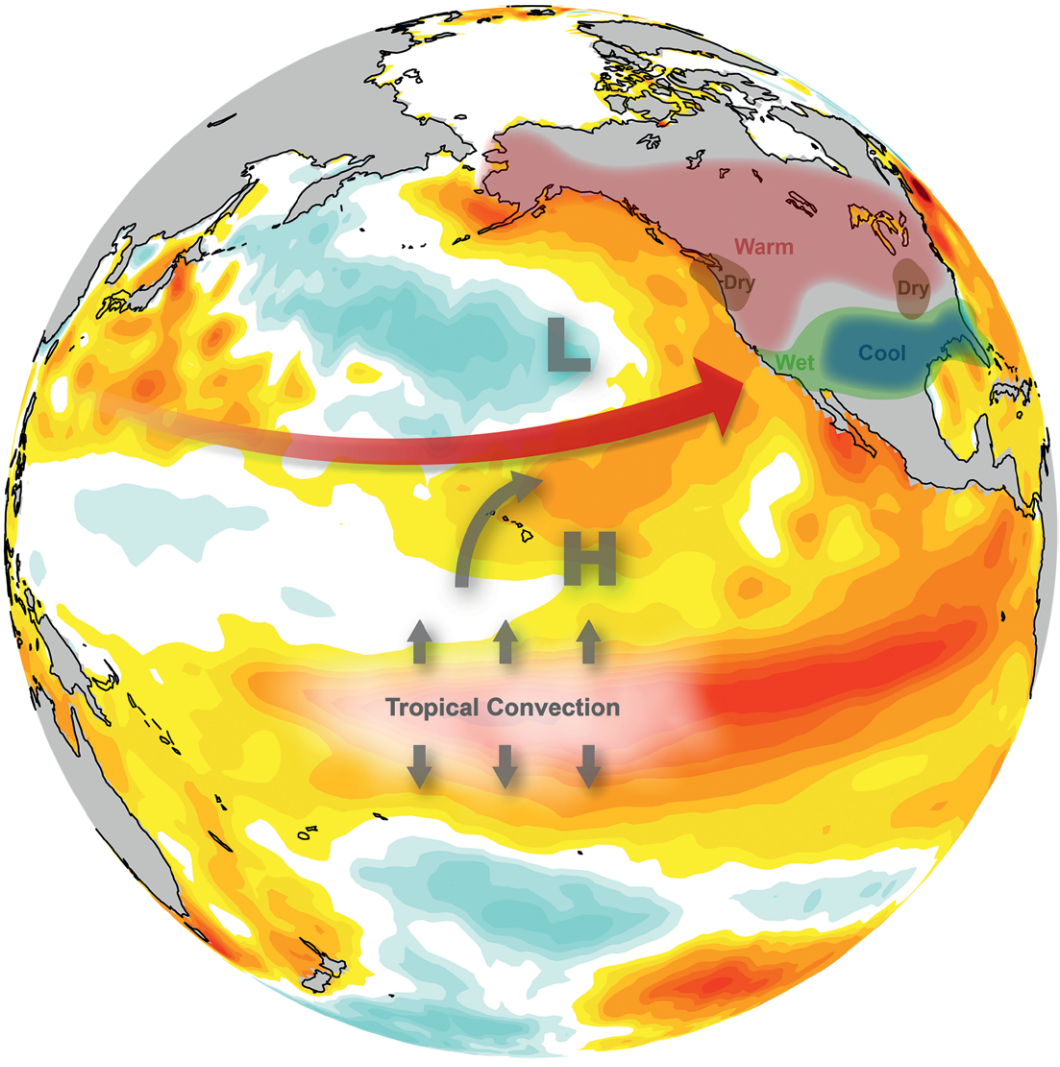


**Fig. 3. Schematic of typical El Niño–related atmospheric processes and phenomena investigated by the ENRR field campaign. Intensified deep convection in the central tropical Pacific (light pink shading) occurs over anomalously warm SSTs related to El Niño (red shading), forcing divergent outflow at upper levels out of the convective region (poleward arrows) with anticyclonic turning in the poleward flow (curved arrow). Outside the tropics, this typically produces a southward-displaced and eastward-extended wintertime jet stream (large red arrow) over the eastern North Pacific, with intensified high pressure (H) south of the jet and low pressure (L) to the north. Altered circulation often continues in a wavelike pattern farther downstream, contributing to weather and climate impacts over North America and globally, illustrated here over land by warm (light red), dry (brown), wet (light green), and cool (blue) conditions compared to normal. SST anomalies shown are for Jan–Mar (JFM) 2016 from the NOAA Optimum Interpolation, version 2 (OI.v2), dataset.**

response. Supporting this objective, PSD and NWS coordinated research and services to ensure that ENRR field campaign observations could be assimilated into operational prediction models while also contributing to research toward advancing scientific understanding and longer-term model improvements. Most actions focused on what NOAA could do; however, PSD scientists also engaged the broader weather and climate community beyond NOAA, including through special sessions organized at American Geophysical Union and American Meteorological Society conferences. These interactions helped NOAA to refine its ENRR plans to serve broader community science objectives.

Planning often proceeded opportunistically. For example, the primary asset for the field campaign over the tropical Pacific was the NOAA G-IV aircraft. Prior to the El Niño predictions, PSD had been allocated 100 hours of G-IV flight time to validate a new wind lidar instrument. Because of development delays, the lidar instrument was unavailable in 2016. Given the El Niño opportunity, PSD reallocated these 100 flight hours for the campaign. A request of 80 additional

| Table 1. NOAA organizational acronyms. | |
|---|---|
| **NOAA line offices** | |
| NESDIS | National Environmental Satellite, Data, and Information Service |
| NOS | National Ocean Service |
| NWS | National Weather Service |
| OMAO | Office of Marine and Aviation Operations |
| OAR | Office of Oceanic and Atmospheric Research |
| **NOAA centers, laboratories, programs, test beds** | |
| AOC | Aircraft Operations Center |
| CPC | Climate Prediction Center |
| CSD | Chemical Sciences Division |
| ESRL | Earth System Research Laboratory |
| HMT | Hydrometeorology Testbed |
| MOC-A | Marine Operations Center–Atlantic |
| NDBC | National Data Buoy Center |
| PSD | Physical Sciences Division |
| SHOUT | Sensing Hazards with Operational Unmanned Technology |

G-IV flight hours was expedited by the NOAA OMAO, with flight hours provided from other parts of NOAA. Such cross-agency coordination and support from all levels of NOAA were essential to achieving an effective agencywide rapid response.

El Niño also provided serendipitous resource opportunities. In 2015, the Atlantic hurricane season had below-normal hurricane activity, consistent with expected suppression of western Atlantic hurricane activity during El Niño (Gray 1984; Bove et al. 1998; Stewart 2016). One impact was that the National Aeronautics and Space Administration (NASA) Global Hawk (GH), a high-altitude long-endurance unmanned aircraft system (UAS), flew fewer hurricane flights than planned within the fall 2015 NOAA SHOUT campaign. The reduction in hurricane flights enabled the UAS program to support three research flights over the extratropical North Pacific concurrent with the ENRR field campaign. These flights focused on oceanic storms and the impact of targeted UAS observations on North American west coast and Alaska forecasts of high-impact weather,

| Table 2. ENRR science questions, hypotheses, and field campaign objectives. Science questions and hypotheses were developed for a broader NOAA ENRR that included concurrent modeling and diagnostic activities as well as the field campaign. Campaign objectives are the specific objectives for the field campaign. |
|---|
| **Science questions** |
| How does tropical convection over the east-central Pacific vary during this event? |
| What are the implications for changes in the subtropical jet structure, Rossby wave activity, and West Coast rainfall? |
| How well do models replicate the convective and dynamical response to El Niño? |
| To what extent are predictions over the United States sensitive to errors emanating from the tropics? |
| What observations and forecast system improvements are required to reduce those errors? |
| **Hypotheses** |
| H1: U.S. West Coast rainfall regimes during this El Niño will be modulated by the intensity, zonal extent, and location of tropical Pacific convection, with higher West Coast rainfall following eastward extension and intensification of convection. |
| H2: Model prediction errors in response to El Niño will result from deficiencies in the representation of physical processes, especially tropical convection, as well as limitations in observations and data assimilation over the tropical Pacific. |
| H3: Prediction models will diverge rapidly from vertical thermal and dynamical structures obtained from high-resolution observations. |
| **Campaign objectives** |
| 1) Determine the atmospheric boundary layer and vertical thermal and wind structures related to El Niño, and assess the adequacy and limitations of NOAA forecast systems in simulating the response to the event. |
| 2) Obtain high-horizontal-resolution and high-vertical-resolution observational data required to estimate tropical convective heating and divergent flow and effects on the subtropical jet and extratropical storm activity. |
| 3) Make the data available in real time for input into NOAA and other global forecast models. |
| 4) Assess forecast system sensitivities to uncertainties in model physics, data assimilation, or observations related to tropical convection. |
| 5) Evaluate satellite retrievals in this otherwise sparsely observed region. |
| 6) Increase NOAA's situational awareness and early warning capabilities in response to this potentially high-impact climate event. |

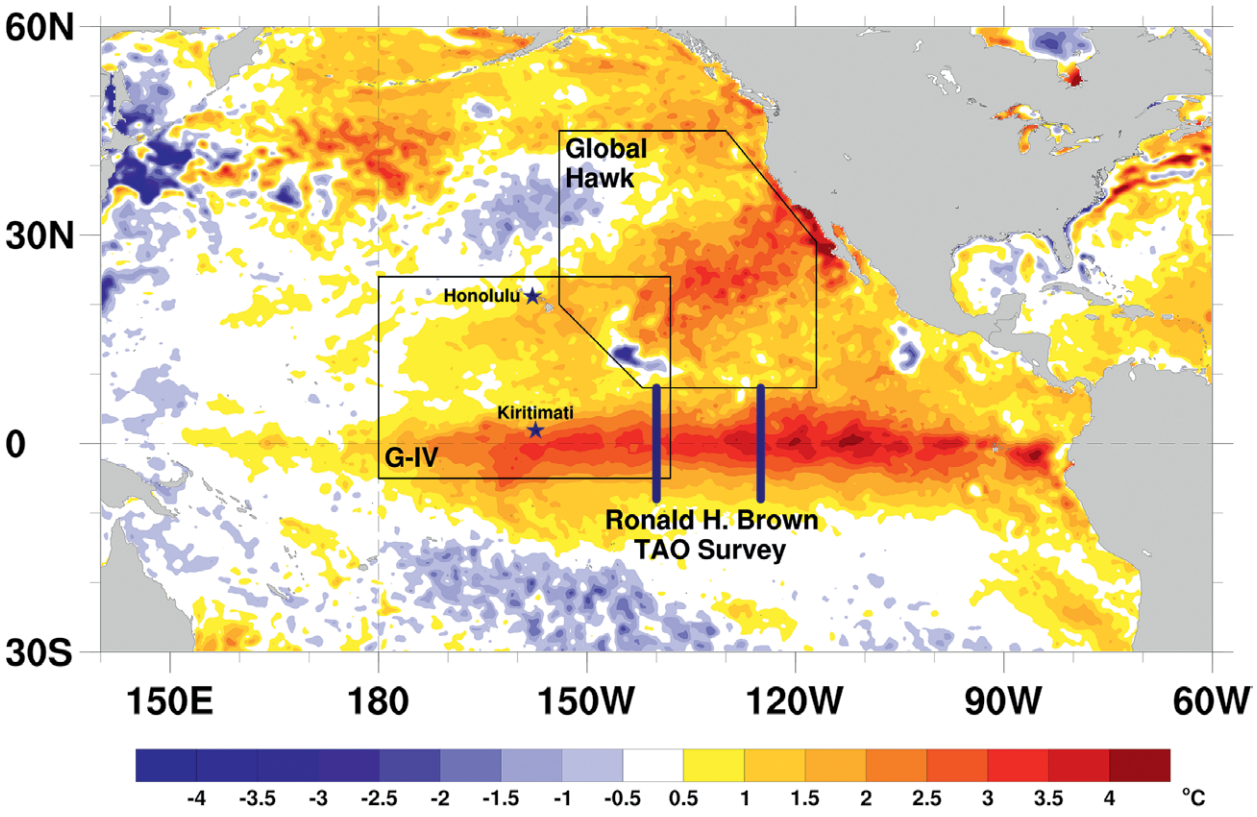


**Fig. 4. Schematic ENRR implementation plan for primary field campaign assets over the tropical and midlatitude North Pacific to the U.S. West Coast. Principal campaign objectives were to obtain observations of i) thermodynamic and dynamic processes near and poleward of convection in the central tropical Pacific (G-IV); ii) subtropical–midlatitude processes and interactions from the eastern North Pacific to the West Coast (GH); and iii) temperature, moisture, and wind profiles from the surface to the middle stratosphere at locations in the central and eastern tropical Pacific (Kiritimati and *RHB*). SSTs shown are from NOAA OI.v2 daily data for 25 Oct 2015.**

consistent with SHOUT program objectives. The participation of the GH and the G-IV established a baseline observational framework for the field campaign that extended from the deep tropics to the U.S. West Coast.

Additional actions further strengthened this core observation strategy. The NDBC had previously planned to service the Tropical Atmosphere Ocean (TAO) array of moorings in the eastern tropical Pacific with the NOAA ship *Ronald H. Brown* (*RHB*) in February–March 2016. PSD scientists joined the cruise to launch radiosondes, providing upper-air coverage during the field campaign over a region mostly beyond flight coverage of the G-IV and GH. NOAA also implemented an expedited international agreement with the Republic of Kiribati to launch radiosondes from Kiritimati (2.0°N, 157.4°W) during the campaign (see "Science and outreach on Kiritimati"). These soundings provided a valuable continuous record of upper-air observations near the warmest El Niño SSTs, complementing the more episodic G-IV flights in the same region.

Observations along the U.S. West Coast coordinated with CalWater-2 field activities (www.esrl.noaa.gov/psd/calwater/; Ralph et al. 2016) provided continuous near-surface-level meteorological measurements from the existing NOAA HMT network (https://hmt.noaa.gov/). An X-band radar installed in Santa Clara, California, during the field campaign helped characterize precipitation distributions throughout the San Francisco Bay area (Cifelli et al. 2018), supporting an end-to-end observational capability extending from processes over the tropical Pacific to West Coast impacts (Fig. 4).

**OVERVIEW OF FIELD CAMPAIGN CONDITIONS.** The ENRR field campaign began 21 January 2016 with the first G-IV research flight and concluded 28 March 2016 with the final radiosonde launch from Kiritimati. Since the campaign was predicated on forecasts for a strong El Niño, a key question is how the conditions during the campaign compared to forecasts and earlier events.

To address this question, Table 3 and Fig. 5 provide overviews of El Niño and large-scale atmospheric

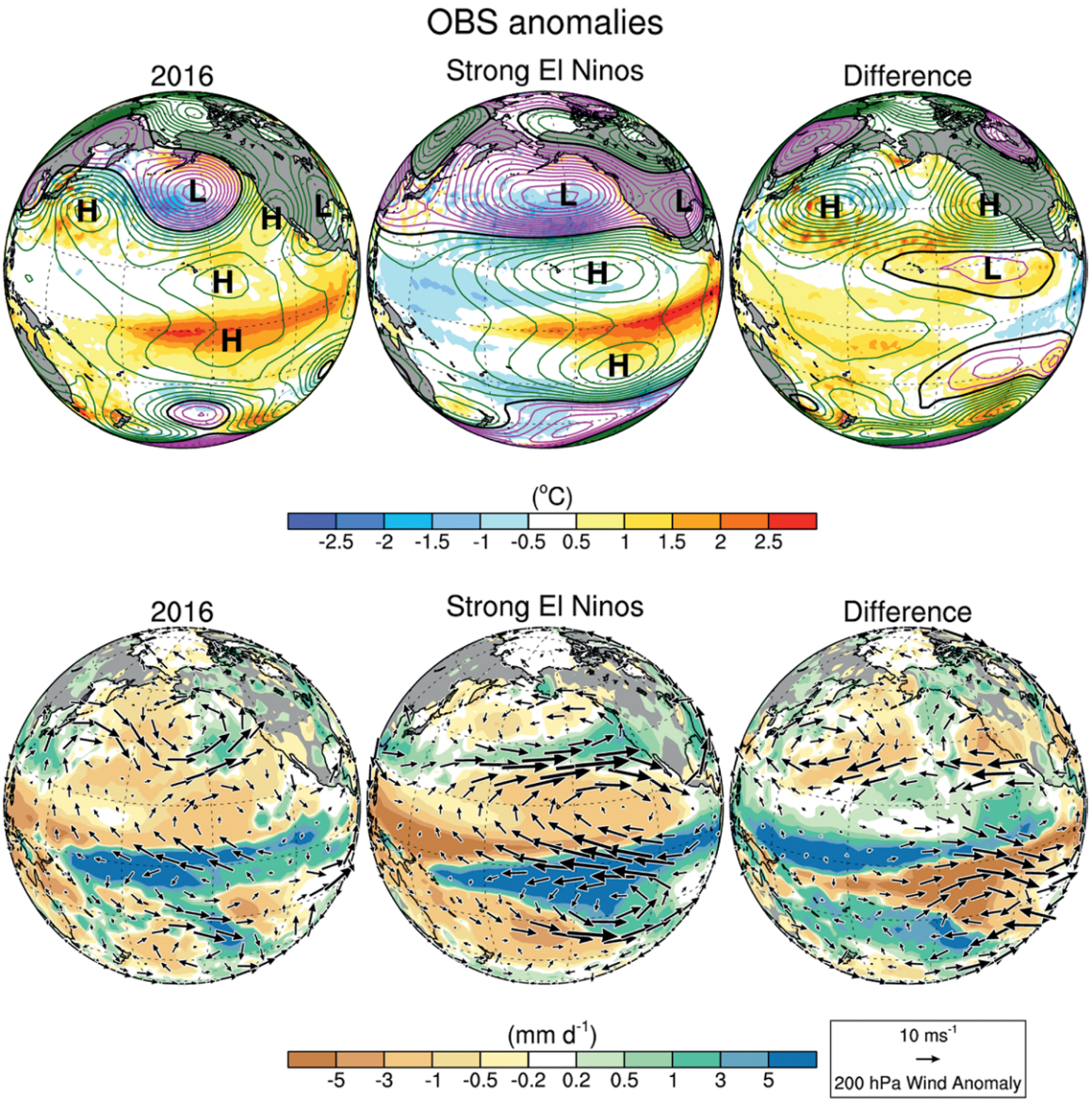


**Fig. 5. (left) Atmospheric anomalies during the ENRR field campaign 19 Jan–28 Mar 2016, (middle) corresponding averages of the two most recent strong El Niño events (1983 and 1998) for the same range of days, and (right) differences. Anomalies are shown (top) for 200-hPa heights (contours, 15 m) and SSTs (shading, 0.5°C) and (bottom) for 200-hPa winds (arrows) and satellite-estimated rainfall (shading, mm day$^{-1}$). [Wind and height fields are from the National Centers for Environmental Prediction (NCEP)–National Center for Atmospheric Research (NCAR) reanalysis, SSTs from the NOAA OI.v2 dataset, and precipitation from the Global Precipitation Climatology Project.]**

conditions during the campaign, respectively. Table 3 compares the strength of 2015/16 El Niño sea surface temperature anomalies to values for the most recent strong El Niño events in 1983 and 1998, for different standard index areas extending across the Pacific. All three events had quite similar amplitudes in the eastern equatorial Pacific, exceeding two standard deviations above normal, consistent with expectations by mid-2015 for a strong El Niño (L'Heureux et al. 2017). However, relative to these two prior events, SST anomalies in 2015/16 were weaker along the South American coast (Niño-1+2) and stronger near the date line (Niño-4). El Niño events vary in several aspects (e.g., Capotondi et al. 2015), and this westward shift (Fig. 5, top) suggests that 2015/16 had more of a "central Pacific" El Niño flavor (L'Heureux et al. 2017), although some of the near-record date line warmth may reflect long-term trends since the early twentieth century (Newman et al. 2018).

The corresponding time-mean atmospheric conditions over the tropical and midlatitude North Pacific during the field campaign (19 January–28 March 2016)

(Fig. 5, left) also resembled the average of the two most recent prior strong events (Fig. 5, middle). Although too small a sample to be considered broadly representative, the 1983 and 1998 events were strikingly similar in many aspects, with their widespread recognition stimulating comparisons to this event in the public and media, as well as among scientists. For both 2016 and the prior events, rainfall was above normal along the equatorial Pacific, spanning almost the entire width of the Pacific basin. East of the date line, enhanced rains were centered near 5°N, whereas farther west enhanced rains were centered near 5°S. An anomalous eastward shift of rainfall associated with the South Pacific convergence zone was a key feature in the subtropical Southern Hemisphere. Upper-troposphere anticyclonic anomalies occurred poleward of the strong positive SST anomalies, being most pronounced in the Northern Hemisphere slightly southeast of Hawaii. Anomalous low pressure prevailed over the North Pacific centered near 45°N, 155°W.

**Table 3. El Niño Dec–Feb (DJF) 2015/16 SST indices compared to two of the recent strongest El Niño events. Indices are determined from area-averaged DJF SST anomalies, relative to 1950–2016, from the Extended Reconstructed SST (ERSST), version 3b, dataset. Anomalies are then standardized with respect to the 1950–2016 period. Regions are defined as follows: Niño-1+2 (10°S–0°, 90°–80°W), Niño-3 (5°S–5°N, 150°–90°W), Niño-3.4 (5°S–5°N, 170°–120°W), and Niño-4 (5°S–5°N, 160°E–150°W).**

| El Niño events | Niño-4 | Niño-3.4 | Niño-3 | Niño-1+2 |
|---|---|---|---|---|
| 1982/83 | 1.1 | 2.2 | 2.8 | 3.2 |
| 1997/98 | 1.2 | 2.2 | 3.0 | 4.3 |
| 2015/16 | 1.9 | 2.3 | 2.6 | 2.3 |

Despite these broad similarities, various 2016 features differed markedly from the prior two events. The difference pattern in rainfall (Fig. 5, right), nearly as intense as the El Niño anomalies themselves,

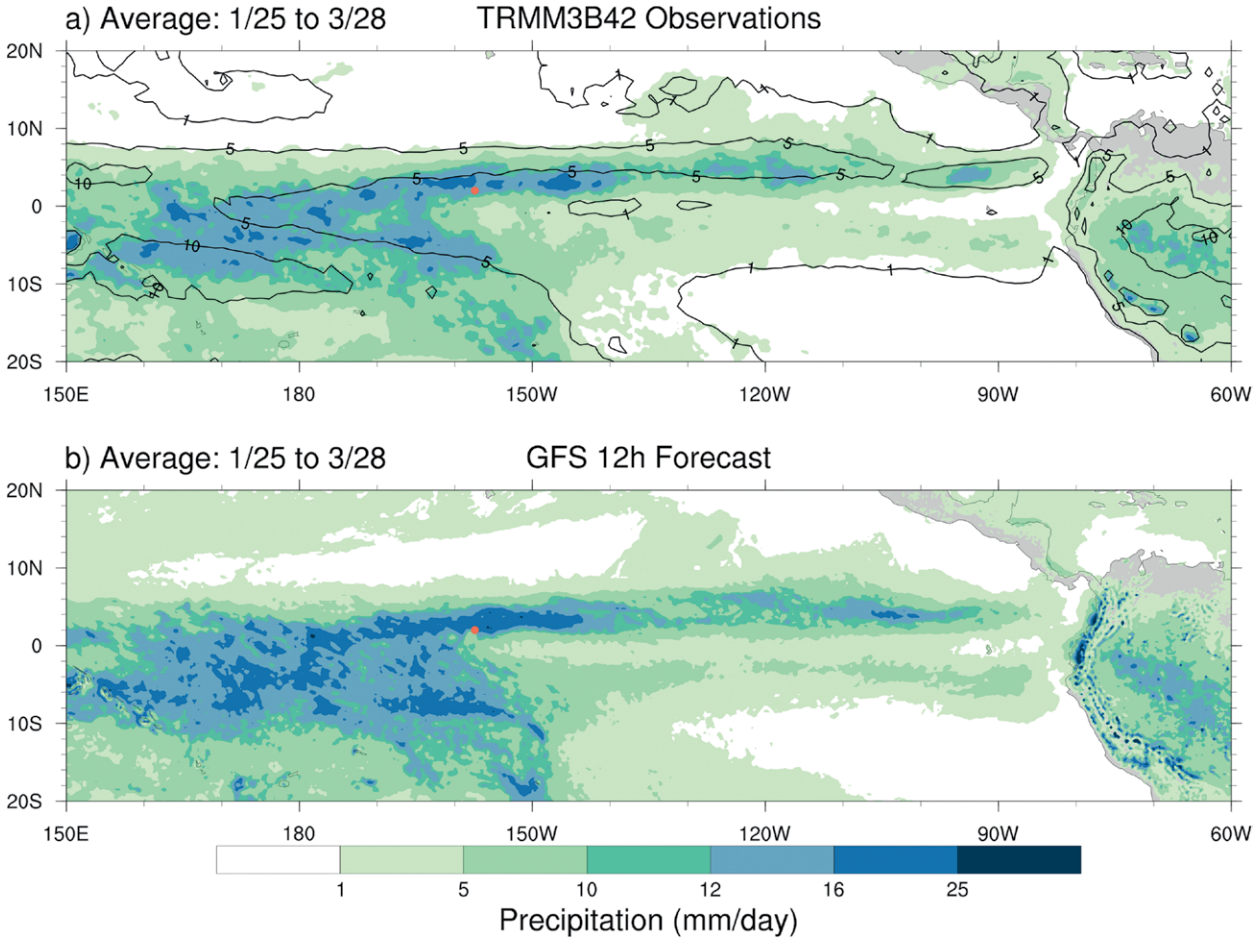


**Fig. 6. Average precipitation (mm day$^{-1}$) over the tropical Pacific from 25 Jan to 28 Mar 2016 from (a) the *Core Observatory* satellite using the Tropical Rainfall Measuring Mission (TRMM) 3B42 algorithm and (b) 12-h NOAA GFS accumulated precipitation forecasts. Contours in (a) depict average values over the same dates from the *Core Observatory* satellite for 1998–2016. Location of CXENRR (orange circle) near 2°N, 157°W is shown.**

## SCIENCE AND OUTREACH ON KIRITIMATI

How do we stimulate interest in learning about science? How do we make the abstract real? One way is to send scientists and engineers, many with no prior field campaign experience, to a remote island in the equatorial central Pacific to collect critical observations during a monster El Niño.

On 25 January 2016, two PSD engineers arrived on Kiritimati (pronounced "Christmas") Island to set up a surface meteorological station and radiosonde launch site outside a two-unit bungalow at the Captain Cook Hotel. For the next two months, that bungalow was both home and "office" for a rotating contingent of NOAA and Cooperative Institute for Research in Environmental Sciences (CIRES) staff members. Their backgrounds were diverse. Some were seasoned field staff, some had analyzed field campaign data for many years but never collected observations, and others specialized in computer modeling or information technology. The primary mission for all was to conduct twice-daily radiosonde launches (0000 and 1200 UTC) and then transfer the data to Boulder, Colorado, as rapidly as possible, for flight planning and for use in operational forecast models run by NOAA and other global modeling centers. Their days were also filled with on-the-ground encounters with El Niño and with opportunities to interact with residents, tourists from around the world, and a wide variety of geoscientists.

On Kiritimati, El Niño dominates interannual rainfall variability, replenishing the freshwater supply that is essential to life on the island. The rain was the big weather story, and it affected everyone. While scientists at home discussed weakening SST anomalies and the end of El Niño, those on Kiritimati knew the SSTs were plenty warm enough for convection. The ITCZ was often parked within view if not directly overhead. Any difficulties in balloon launches during squalls or navigating flooded paths were compensated for by plentiful drinking water and unrestricted showers.

The observers had many opportunities to interact with Kiritimati residents and others from around the world. Several assisted with launches. One local school teacher wished to give his students firsthand exposure to the science he was teaching, which resulted in two groups of 35–40 "third form" (13-year-old) students and their teachers participating in a balloon launch (Fig. SB1) and meeting with our observers. Other residents and visitors to Kiritimati were also eager to learn more about El Niño and the campaign. All these interactions, as well as life on this remote atoll, were educational to the observers and profoundly affected many. Descriptions of their experiences and impressions from Kiritimati are available on the CIRES ENRR blog (http://ciresblogs.colorado.edu/el-nino-rapid-response/). These stories from the field can serve as a resource for students and adults interested in learning more about El Niño and meteorological field work, thereby extending the educational experiences that began on this remote atoll in the central tropical Pacific.

describes a westward and mostly northward shift in enhanced rainfall during the period. Owing to this difference, the region of enhanced convection targeted during the campaign was consistently reachable by Hawaii-originating flights. In what appears to be a dynamically consistent circulation response to the westward shift (compared to the prior two strong El Niño events), anomalous subtropical twin anticyclones were less zonally expansive over the eastern Pacific. Less clear is whether the substantially weaker and less zonally expansive North Pacific cyclonic anomaly in 2016 was driven by the unique aspects of tropical Pacific rainfall patterns.

Figure 6 depicts the time-mean precipitation over the tropical Pacific during the campaign. NASA Global Precipitation Measurement (GPM) *Core Observatory* satellite data (Fig. 6a) show a large-scale eastward shift of tropical Pacific precipitation and an active intertropical convergence zone (ITCZ) with enhanced rainfall and convection in the central Pacific north of the equator, as expected with El Niño, with a maximum almost due south of Hawaii. In comparison, the NOAA Global Forecast System (GFS) 12-h accumulated precipitation forecast totals (Fig. 6b) show relatively stronger and westward-shifted maxima, the double ITCZ in the eastern tropical Pacific is overly enhanced, and there is more widespread very light precipitation than estimated by the *Core Observatory*.

On average, Kiritimati was on the southern edge of the ITCZ. The expected strong enhancement of Kiritimati rainfall was confirmed by ENRR special observations at station CXENRR (Kiritimati) and supported by a second gauge, Decca, about 8 km away [Fig. 7; Table 4; map with locations is shown in the online supplement (https://doi.org/10.1175/BAMS-D-16-0219.2)]. CXENRR recorded 938 mm in nine weeks, nearly the 1951–2015 annual average of 1,027 mm (T. Falkland 2016, personal communication). The CXENRR observations were within 10% of and well correlated with measurements at other island sites 6–8 km away (Fig. 7; see supplement). Model predictions are shown at two lead times, 12 and 48 h, used for determining specific targets and flight plans that day and planning sequences of flights and potential targets in subsequent days.

**Fig. SB1. ENRR meteorologist Leslie Hartten helping a student from Thompson Ramo Wooldridge Junior-Secondary School on Kiritimati launch the 0000 UTC radiosonde on 27 Mar2016. Another student (to right in patterned shorts) had helped release the balloon from the tarpaulin tube in which it had been filled. In the background are two-unit bungalows resembling the one ENRR staff lived and worked out of during the field campaign. (Photo credit: G. Kerber.)**

As shown in the figure and table, about two-thirds of the observed rain fell during six major events. *Core Observatory* precipitation estimates during deployment totaled 84% of observed and captured the occurrence but not magnitude of most large events. Total rain from interpolated GFS 48-h and Integrated Forecast System (IFS) 12- and 48-h forecasts were generally lower than observed. One 299-mm extreme event forecast by the 12-h GFS that failed to occur helped push its campaign period total above the largest island-based value. The models did a generally poor job of capturing the major rain events, with the IFS 48-h forecasts displaying less variation in rainfall intensity than observed.

As in previous El Niño events, subseasonal convective variability was prominent during the field campaign. Figure 8 illustrates the evolution of daily averaged equatorial convection anomalies for the 1983, 1992, 1998, and 2016 El Niño events, each separated into its El Niño (contours) and intraseasonal (shading) components using the technique of Newman et al. (2009). While the eastern Pacific El Niño response in 2016 was centered between 150° and 165°W, as in past events, it was weaker than in previous strong events. Figures 8 and 9a also show that during strong El Niño events, equatorial convection undergoes substantial synoptic variability dominated by eastward-propagating convectively coupled waves, including Kelvin waves (Kiladis et al. 2009). In turn, these waves modulate mesoscale convective systems (MCSs) propagating both westward and eastward within larger-scale envelopes, as seen in Fig. 9a.

This precipitation variability posed major challenges to forecast models, particularly the GFS, affecting flight operations and planning. Figure 9 shows tropical Pacific precipitation rate estimates from *Core Observatory* satellite data compared with 12- and 48-h quantitative precipitation forecasts (QPFs) from the GFS and IFS. The satellite data depict large-scale precipitation features propagating both eastward and westward across the tropical Pacific throughout the campaign period, substantially modulating precipitation variability in the flight operation region. Several of these events were well sampled during the campaign. Figures 9b and 9c show the GFS and IFS 12-h QPF valid for the same times in Fig. 9a. The

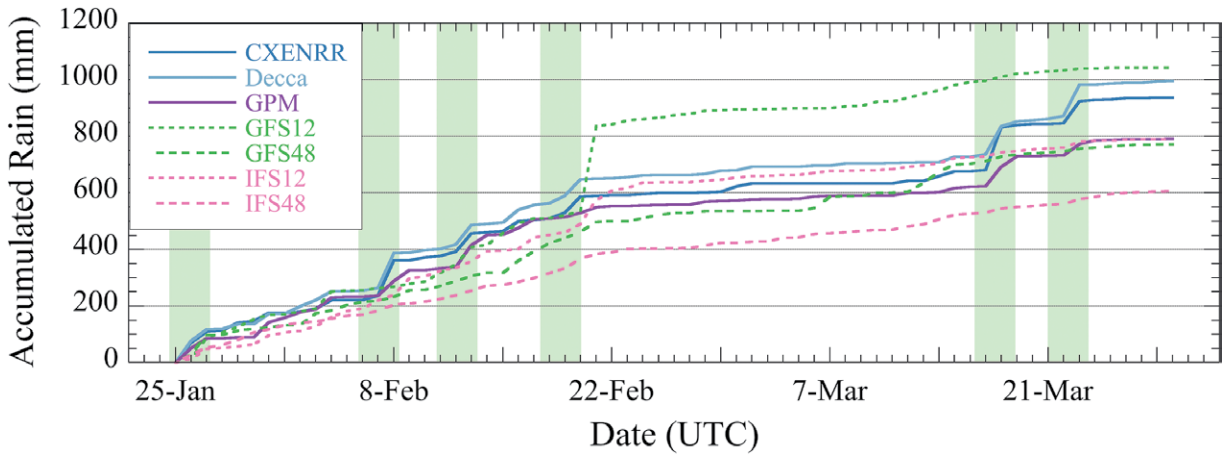


**Fig. 7. Time evolution of accumulated rainfall from observations and forecasts (mm) on Kiritimati during the ENRR field campaign. Values are obtained from rain gauges at CXENRR (blue solid) and Decca (light blue solid), *Core Observatory* satellite–based estimates from the TRMM 3B42 algorithm interpolated to the location of CXENRR (purple solid), and 12- and 48-h forecasts from the NOAA GFS (green small dash and green large dash, respectively) and ECMWF IFS (pink small dash and green large dash) interpolated to the location of CXENRR. GFS and IFS were run at native resolutions of 13 and 16 km, respectively. *Core Observatory*, GFS, and IFS values were all interpolated to CXENRR's location using inverse distance weighting from surrounding (0.25° resolution) grid points. All precipitation was summed over UTC days. Light green vertical bars indicate major rain events occurring concurrently in all available ground-based observations (see supplement) and usually extending over two consecutive days.**

ability of both forecast systems to reproduce many of the same features in Fig. 9a is impressive, especially since precipitation data are not directly assimilated into either system, highlighting the effectiveness of the assimilation of wind and thermodynamic fields. However, the GFS especially shows a degradation of the finer-scale features when compared to the IFS, along with more widespread light precipitation that is not present in the satellite estimates. By 48 h there is a rapid degradation of the QPF in both systems (Figs. 9d and 9e), although the ability of the models to maintain propagating features is noticeably better in the IFS.

**Table 4. Observed and model forecast rainfall on Kiritimati during the ENRR deployment on Kiritimati, 25 Jan–28 Mar 2016. Observations are from tipping buckets at the ENRR site (CXENRR) and the Decca site (2.04°N, 157.47°W), and from the *Core Observatory* satellite (3-h accumulations using the TRMM 3B42 algorithm; 0.25° gridding, linearly interpolated to 2.01°N, 157.4°W). Forecasts are 6-h accumulations from the GFS and IFS at 12- or 48-h leads, 0.25° gridding interpolated to 2.01°N, 157.4°W.**

| | Observations | | | Forecasts | | | |
|---|---|---|---|---|---|---|---|
| | CXENRR | Decca | *Core Observatory* | GFS12 | GFS48 | IFS12 | IFS48 |
| **Total rainfall (mm)** | 938 | 996 | 791 | 1,044 | 772 | 792 | 606 |
| **Diff from CXENRR (%)** | | +6 | −16 | +11 | −18 | −16 | −35 |
| **Diff from *Core Observatory* (%)** | +19 | +26 | | +32 | −2 | 0 | −23 |
| **Rainfall (mm) during major events** | | | | | | | |
| **26–27 Jan 2016** | 110 | 118 | 86 | 88 | 98 | 49 | 54 |
| **7–8 Feb 2016** | 140 | 133 | 57 | 13 | 18 | 47 | 35 |
| **12–13 Feb 2016** | 81 | 85 | 83 | 91 | 36 | 34 | 30 |
| **19–20 Feb 2016** | 77 | 84 | 21 | 26 | 38 | 38 | 52 |
| **18–19 Mar 2016** | 160 | 116 | 107 | 24 | 23 | 19 | 20 |
| **23–24 Mar 2016** | 83 | 111 | 54 | 7 | 13 | 23 | 23 |
| **Major event subtotal (mm)** | 652 | 646 | 407 | 251 | 226 | 210 | 215 |
| **Percentage of total** | 69% | 65% | 51% | 24% | 29% | 27% | 35% |

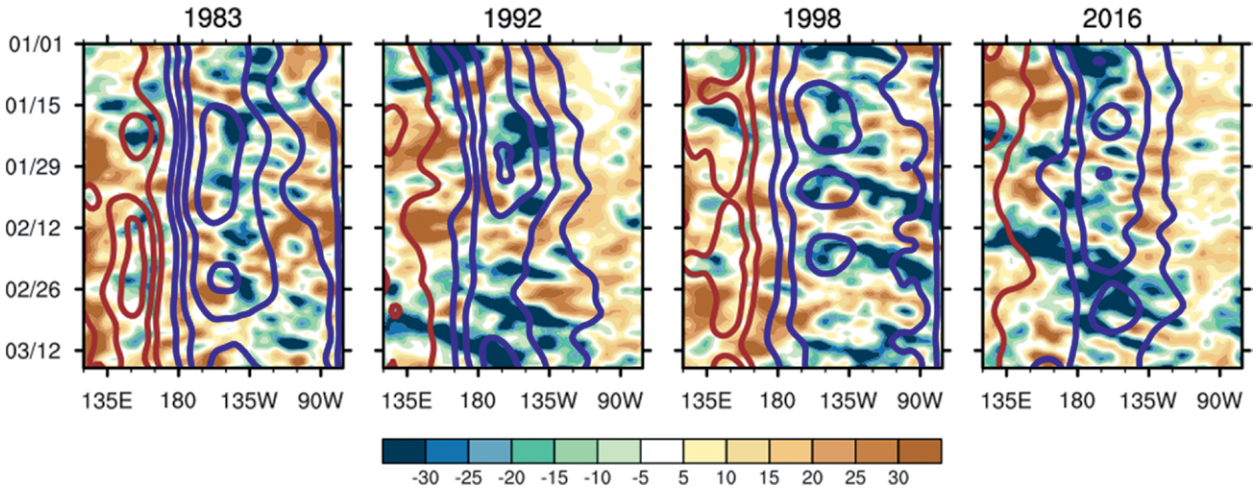


**Fig. 8. El Niño and intraseasonal components of outgoing longwave radiation (OLR) as shown in Hovmöller diagrams, averaged between 5°S and 5°N, of daily OLR anomalies across the equatorial Pacific. Both components are shown for the El Niño events of 1983, 1992, 1998, and 2016. Contours (15 W $m^{-2}$ interval, negative values in blue) indicate the El Niño component; shading (5 W $m^{-2}$ interval) indicates the remaining intraseasonal component, including eastward-propagating Madden–Julian oscillation and equatorial Kelvin waves. Total OLR anomaly is the sum of the two fields.**

Similar comparisons for longer lead times (not shown) indicate systematic drift of the model precipitation away from its observed location. We are carrying out a detailed quantitative analysis of the GFS and IFS QPF and dynamical fields, and those results will be reported in future studies.

The previous analyses strongly emphasize the importance of subseasonal variability in precipitation over the tropical Pacific during El Niño. Figures 7 and 9 further suggest deficiencies in model representations of this variability. The relationships between higher-frequency precipitation variability and more slowly varying El Niño conditions were crucial to ENRR field campaign operations. Whether they also played a significant role in the extratropics in 2016 is the subject of ongoing research.

**ENRR FIELD CAMPAIGN IMPLEMENTATION.** On 19 January 2016, the G-IV arrived in Honolulu, Hawaii, and PSD initiated daily weather briefings led by its scientists, with additional contributions provided by many others in NOAA and the external community (see "Role and value of daily weather briefings"). The first G-IV research flight occurred on 21 January, with other facilities and observing efforts following between late January and mid-February (Table 5). Table 6 provides the dates and primary objectives for all GH and G-IV research flights. Over 50 consecutive weather and flight planning daily briefings occurred through 10 March 2016, concluding with a final G-IV science-in-transit flight back to the U.S. West Coast. Radiosonde campaigns on the *RHB* and in Kiritimati continued through mid- and late March, respectively.

*Operational overview.* G-IV FLIGHT OPERATIONS. The G-IV research aircraft conducted 22 science flights during the field campaign (Fig. 1), with 607 successful dropsonde releases obtaining detailed thermodynamic, moisture, and wind profiles. G-IV flights focused primarily around and poleward of enhanced convection to the south of Hawaii within 1,500 km east or west of Kiritimati (flight tracks are shown in Fig. 1). The G-IV typically conducted 7- to 8-h missions between about 2000 and 0400 UTC [1000 and 1800 Hawaii–Aleutian standard time (HST)], centered around 0000 UTC to optimize the data availability for the 0000 UTC forecast model initialization. The aircraft operated at flight levels between approximately 12.5 and 13.7 km with a meteorological payload of dropsondes and a tail Doppler radar (TDR). On average, 30 dropsondes were launched per flight, each providing high-vertical-resolution temperature, relative humidity, pressure, and wind speed and direction measurements from just below flight level to the ocean surface. The TDR measured reflectivity laterally and below the aircraft, enabling the derivation of three-dimensional winds in precipitating environments after postprocessing.

G-IV flight planning used meteorological satellite data, derived products, and model overlays on planned and actual flight tracks. The NASA Mission Tool Suite (MTS) provided an integrated platform for

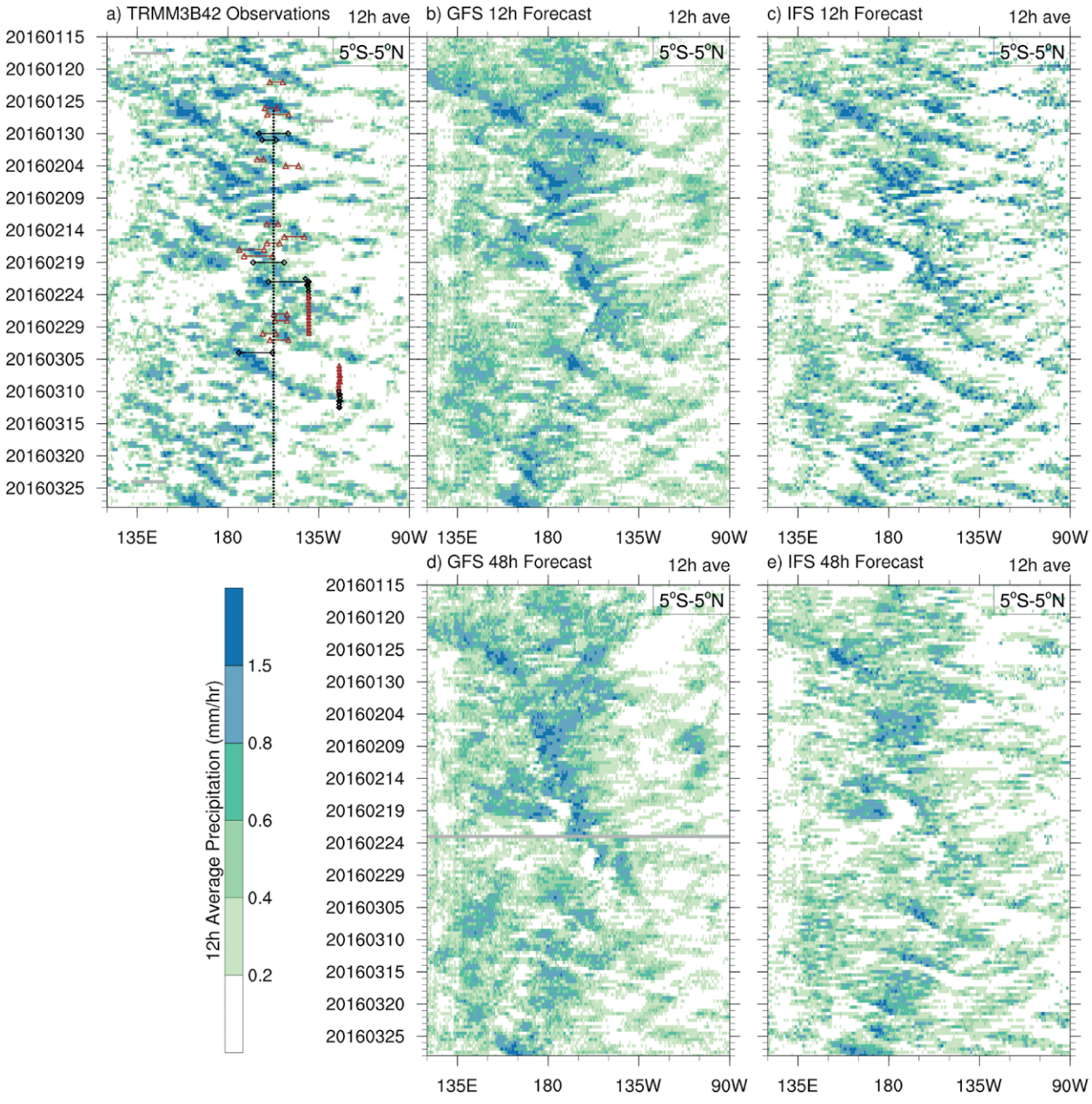


**Fig. 9. Hovmöller diagrams of the time evolution of precipitation (mm $h^{-1}$) averaged between 5°S and 5°N during the ENRR field campaign of (a) satellite-based estimates from *Core Observatory* using the TRMM 3B42 algorithm and for model forecasts at different lead times: (b) GFS 12-h forecast, (c) IFS 12-h forecast, (d) GFS 48-h forecast, and (e) IFS 48-h forecast. Also shown in (a), G-IV dropsonde longitudes (horizontal lines) for drops that were located between 5° and 10°N (green) and south of 5°N (red), the longitude and time of radiosonde measurements on Kiritimati (black dots), and the longitudes and times of radiosonde measurements from *RHB* (crosses) for launches between 5° and 10°N (green) and south of 5°N (red). GFS 48-h panel shows missing data on 24 Feb 2016 (light gray horizontal bar).**

flight plan development and real-time flight guidance. NESDIS contributed real-time temperature and moisture retrievals from the Cross-Track Infrared Sounder (CrIS) and Advanced Technology Microwave Sounder (ATMS) instruments on the *Suomi National Polar-Orbiting Partnership* (*Suomi-NPP*) satellite, using the NOAA Unique Combined Atmospheric Processing System (NUCAPS) (Gambacorta et al. 2013, 2015; Nalli et al. 2018), to inform sampling strategies. G-IV dropsonde observations were processed and quality controlled on the aircraft in near–real time using Atmospheric Sounding Processing Environment (ASPEN) software (Earth Observing Laboratory 2017), and the data transmitted to the

## ROLE AND VALUE OF DAILY WEATHER BRIEFINGS

From launch to landing, a flight mission control center at PSD actively tracked and surveyed the state of weather over the tropical Pacific. Nine flat-screen monitors filled a wall, each animated with the motions of clouds, winds, and storms. Some looped satellite data, while others were used to anticipate conditions over the next several hours to the next several days. This formed a "Weather War Room," where scientists, early career and more senior, were sequestered (Fig. SB2). These were mostly researchers, many having never participated in a field campaign, whose notion of a "rapid response" was measured by the many months needed to complete a research project and publish results. Their normal day jobs included studying atmospheric dynamics and physics and methodically determining what gives birth to storms and how to better measure and predict them, at least theoretically. For many, the tropics were familiar, but some were more accustomed to other remote environments, like the Arctic. Nonetheless, each scientist brought unique insights and knowledge, and each learned.

For what purpose did the scientists gather daily from mid-January through mid-March 2016? Not to debate practical or esoteric theories of weather and climate—that luxury of academics had to (mostly) await another day. No, it was to provide expert guidance for NOAA's daily flight mission into the "teeth of El Niño." Together with the NCEP and NESDIS team members, who remotely provided their unique operational modeling and satellite perspectives, they pored over observed and predicted conditions in the central tropical Pacific for the next two days and judged forecasts from the tropics to North America to inform longer-term flight planning and coordination for the next two weeks. The complexity of the weather challenged most, and humbled all. As synoptic experience was acquired, strengths and weaknesses of guidance from a variety of forecast models were better appreciated, and more refined information was rendered. The mission of the scientists, for which they had all gladly volunteered with excitement and expectation of new knowledge, was to determine how best to guide the G-IV from Hawaii southward to near the equator and back home again on its nearly 8-h flight: Which paths to take, which days to fly, when to rest and regroup—those were the practical matters. Based on the scientists' interpretation of diverse data flashing before their eyes, their first concern was always to ensure safety for flights that carried not only aviation and engineering experts but also their peers and friends. Often those flight missions also met their second objective: to return with measurements of winds, clouds, and moisture that might ultimately unravel mysteries of El Niño and its impacts on weather.


**Fig. SB2. ENRR forecast team members in the Weather War Room.**

**Table 5. ENRR field campaign observational platforms and data availability. STC = Science and Technology Corporation; HRD = Hurricane Research Division; AVAPS = Airborne Vertical Atmospheric Profiling System; SFMR = Stepped Frequency Microwave Radiometer; HAMSR = High-Altitude Monolithic Microwave Integrated Circuit (MMIC) Sounding Radiometer; HIWRAP = High-Altitude Imaging Wind and Rain Airborne Profiler; EOL = Earth Observing Laboratory; JPL = Jet Propulsion Laboratory; GSFC = Goddard Space Flight Center.**

| Platform/ site | Observing period | Theater of operations | Platform lead | Instrument | Instrument type | Instrument lead | Measurement parameters |
|---|---|---|---|---|---|---|---|
| NOAA G-IV/ Honolulu | 19 Jan–11 Mar 2016 | 22 research flights, 628 dropsondes, 38°N–1°S, 180°–120°W | R. Dole (CIRES and NOAA/PSD) and R. Spackman (STC and NOAA/PSD) | AVAPS | Dropsonde system, RS92, RD94 | NOAA/AOC | Vertical profiles of atmospheric pressure, temperature, moisture, GPS winds, and position |
| | | | | TDR | X-band scanning tail Doppler radar | NOAA/AOC | Vertical profiles of reflectivity and wind speed and direction in precipitating environments |
| | | | | SFMR | Stepped Frequency Microwave Radiometer | NOAA/AOC | Near-surface wind speed and temperature over the ocean |
| NASA GH/ Edwards Air Force Base | 2–23 Feb 2016 | 3 research flights, 90 dropsondes, 47°–13°N, 170°–120°W | G. Wick (NOAA/PSD) and J. Dunion (NOAA/HRD) | AVAPS | Mini-dropsonde system, RS92, NRD94 | T. Hock (EOL, NCAR) | Vertical profiles of atmospheric pressure, temperature, moisture, GPS winds, and position[1] |
| | | | | HAMSR | Multichannel sounding radiometer | B. Lambrigtsen (NASA JPL) | Vertical profiles of temperature, moisture, and liquid water |
| | | | | HIWRAP | Ku- and Ka-band scanning Doppler radar | G. Heymsfield (NASA GSFC) | Vertical profiles of reflectivity, precipitation, derived wind speed and direction in precipitating environments, and ocean surface wind speed |
| | | | | UAS ozone | Ozone absorption photometer | T. Thornberry (CIRES and NOAA/CSD) | Ozone mixing ratio |
| NOAA ship *RHB*/ Honolulu to San Diego | 16 Feb–16 Mar 2016 | TAO survey, 29°N–8.0°S, 158°–119°W | D. Wolfe and C. Cox (CIRES and NOAA/PSD) | 193 radiosondes | Vaisala RS92-SGP | D. Wolfe (CIRES and NOAA/PSD) | Vertical profiles of atmospheric pressure, altitude, temperature, moisture, GPS winds, and position[2] |
| | | | | Surface meteorology | Various | NOAA/MOC-A | Pressure, temperature, relative humidity, wind, downwelling shortwave radiation, 5-m ocean temperature, plus others listed on PSD ENRR web page[3,4] |
| | | | | Surface flux | Various | NOAA/MOC-A | Bulk surface energy fluxes and 10-m neutral stability parameters[4,5] |
| | | | | CTD (33) | Sea-Bird SBE 911plus | NOAA/MOC-A | Vertical profiles of oceanic conductivity and temperature[6] |
| Kiritimati | 25 Jan–28 Mar 2016 | 2.01°N, 157.40°W | L. Hartten and P. Johnston (CIRES and NOAA/PSD) | 125 radiosondes | Vaisala RS92-SGP | P. Johnston (CIRES and NOAA/PSD) | Vertical profiles of atmospheric pressure, altitude, temperature, moisture, GPS winds, and position[7] |
| | | | | Surface meteorology | Various | P. Johnston (CIRES and NOAA/PSD) | Pressure, temperature, relative humidity, wind, and precipitation[8] |

**Table 5. Continued.**

| Platform/ site | Observing period | Theater of operations | Platform lead | Instrument | Instrument type | Instrument lead | Measurement parameters |
|---|---|---|---|---|---|---|---|
| Santa Clara | Jan–May 2016 | 37.39888°N, 121.83340°W | R. Cifelli (NOAA/ PSD) | X-band radar | Ground-based dual-polarization radar | R. Cifelli (NOAA/ PSD) | Reflectivity and rainfall rates |
| *Suomi-NPP* satellite | Continuous | Low-Earth orbit | C. Barnet (STC and NESDIS) | CrIS | Cross-Track Infrared Sounder | NESDIS | NUCAPS retrievals of vertical profiles of temperature and moisture |
| | | | | ATMS | Advanced Technology Microwave Sounder | NESDIS | |

[1] Earth Observing Laboratory (2016).
[2] Cox et al. (2017a).
[3] Cox et al. (2017b).
[4] See www.esrl.noaa.gov/psd/enso/rapid_response/data_pub/.
[5] Cox and Hartten (2017).
[6] Wolfe et al. (2017).
[7] Hartten et al. (2017b).
[8] Hartten et al. (2017c).

Global Telecommunication System (GTS) for use in operational numerical weather predictions.

The preferred flight sampling strategy, the "convective enclosure module" (orange flight tracks in Fig. 1), was designed to enclose convective complexes extending over several degrees of latitude and longitude to determine their thermodynamic and wind environments and associated physical and dynamical processes. The flights took advantage of the TDR to map out precipitation in convective towers, yielding three-dimensional wind speed and direction after postprocessing. Convective enclosure flight plans were difficult to execute because of safety concerns related to widespread deep convection and limited skill in forecasting the location and evolution of the complexes. Nevertheless, the campaign successfully conducted 10 convective enclosure flights.

An alternative strategy, the "convective outflow module" (red flight tracks in Fig. 1), instead made measurements in data-sparse regions just north of the convection, focusing on the intensity and vertical structure of poleward upper-level outflow that is vital in linking El Niño to higher-latitude impacts. This approach, employed in almost half of the research flights, sampled longer zonal swaths than possible in the convective enclosure flights, typically 10° longitude or longer.

A final series of flights over a weeklong period in early March tracked a cascade of dynamical processes from the tropics to the U.S. West Coast. These flights involved a coordinated mission between the G-IV and the NASA Ames–directed Alpha Jet while an atmospheric river was making landfall in Northern California (see "Tropical–extratropical linkages").

Radiosonde observations. Complementing the G-IV observations in this sparsely sampled region of the Pacific, radiosondes were launched twice daily from Kiritimati and up to eight times daily from the *RHB*. Radiosonde launches at 0000 and 1200 UTC began on Kiritimati on 25 January 2016 and continued through 28 March 2016 (Hartten et al. 2017a, 2018). The 0000 UTC launches (1400 LT) complemented observations from the G-IV, which was often nearby at this time, as well as *Suomi-NPP* satellite overpasses with equatorial crossings at 1330 and 0130 LT.

The *RHB* sailed from Honolulu on 16 February 2016 to service TAO buoys along 140° and 125°W between 8°N and 8°S, arriving into port in San Diego, California, on 16 March 2016. A total of 193 radiosondes were successfully launched during the cruise. The most intensive observations were performed in the data-void region along the buoy service lines in

the deep tropics (Fig. 4). While en route, the *RHB* launched radiosondes on 17, 18, and 21 February coordinated with contemporaneous G-IV dropsonde releases for intercomparison purposes.

Global Hawk flight operations. During the ENRR field campaign, three flights with the GH over the eastern Pacific were conducted by the NOAA UAS program SHOUT project (Wick et al. 2018). The payload consisted of dropsondes and other advanced instrumentation (Table 5). The GH primarily focused on targeted extratropical observations to impact North American west coast and Alaska storm forecasts. When feasible, G-IV operations were scheduled to coincide with GH flights to maximize the coverage of simultaneous eastern Pacific tropical and extratropical observations. The GH science flights (green dashed tracks in Fig. 1) of up to 24 h in duration were conducted between about 16.5 and 19 km in February 2016, deploying a total of 90 dropsondes. These GH and G-IV flights were coordinated with two C-130 aircraft from the 53rd Weather Reconnaissance Squadron, which conducted six research flights focusing on atmospheric rivers between Hawaii and the U.S. West Coast.

*Data processing and availability.* ENRR field campaign datasets were derived from five primary platforms and one auxiliary observing platform (Table 5). The PSD website (www.esrl.noaa.gov/psd/enso/rapid_response/data_pub/) provides links to the latest versions of these datasets as well as essential information, sample plots, and code to utilize them effectively. Data on the site are freely available to the research community and the public. Data not already archived elsewhere will be archived at the National Centers for Environmental Information (NCEI) but will continue to be linked on the PSD ENRR data web page. More details on data processing, metadata, and quality control are provided in the supplement.

In addition, data of opportunity and supporting products are also available. Among these are temperature and salinity from conductivity–temperature–depth (CTD) instruments deployed by the *RHB*, 6-hourly surface pressure analyses over the North Pacific, historic wind profiler data from the Trans-Pacific Profiler Network (Gage et al. 1991), and HMT-West measurements of surface meteorological variables and wind profiler data along the U.S. West Coast. Additional products will be made available as they are produced.

**EARLY RESULTS.** The field campaign observations are being used now in several studies addressing ENRR questions, hypotheses, and objectives, with additional studies expected. Here we show a few preliminary results that have stimulated more extensive research to assess model forecast systems as well as the impacts of campaign observations on model analyses and forecasts.

*ENRR dropsondes, satellite, and GFS model comparisons.* A specific campaign objective was to obtain observations to evaluate satellite retrievals (i.e., satellite soundings) and satellite-derived model analyses over the central and eastern tropical Pacific, a vast area with few in situ observations. In this region, satellite observations play a predominant role in determining the quality of model-based analyses and subsequent model forecasts. Understanding the impact of available satellite data in this region therefore contributes to longer-term improvements in the model prediction system. In situ dropsonde and radiosonde observations have proven critical for satellite retrieval validation as well (Nalli et al. 2013, 2018). Note that satellite retrievals use more satellite data than can be assimilated into the model-based analysis.

Figure 10 shows latitude–height plots from 0° and 20°N of two key variables, equivalent potential temperature $\theta_e$ and specific humidity $q$, derived from the G-IV flight dropsonde data (Fig. 10a), compared with *Suomi-NPP* satellite-retrieved NUCAPS soundings and interpolated GFS model analysis and forecast fields. The analyses are displayed as averages over all flight days and longitudes between 162° and 150°W. All three datasets have

**Table 6. ENRR flight dates and primary objectives.**

| G-IV convective enclosure | G-IV convective outflow | G-IV tropical–extratropical | GH extratropical |
|---|---|---|---|
| 21 Jan | 25 Jan | 6 Mar | 12–13 Feb |
| 26 Jan | 29 Jan | 8 Mar | 15–16 Feb |
| 2 Feb | 30 Jan | 10 Mar | 21–22 Feb |
| 3 Feb | 14 Feb | | |
| 12 Feb | 16 Feb | | |
| 15 Feb | 17 Feb | | |
| 26 Feb | 18 Feb | | |
| 27 Feb | 21 Feb | | |
| 29 Feb | 3 Mar | | |
| 1 Mar | | | |

A fundamental observing strategy of ENRR was to examine the dynamical linkages between the tropics and extratropics initiated by large-scale tropical convection associated with El Niño. The final series of three G-IV flights (yellow tracks in Fig. 1) followed the cascade of linked processes downstream over a 5-day period culminating with a high-impact precipitation event along the U.S. West Coast in early March 2016. The first flight examined a tropical moisture export event to the southwest of Hawaii. The intermediate flight probed the related emerging atmospheric river (AR) northeast of Hawaii with the G-IV releasing dropsondes around a large-scale budget box oriented across the moisture flux in the AR.

The final flight in the sequence was conducted as science in transit back to the U.S. West Coast, with the G-IV deploying 42 dropsondes in five transects across the then-mature AR making landfall in the San Francisco Bay area (see Fig. SB3). Valuable data were also acquired with the tail Doppler radar across the more northern reaches of the AR, providing additional interpretive context for the dropsonde data. In coordination with the last G-IV flight, the NASA-directed AJAX (Hamill et al. 2016) launched from Moffett Field, California, while the precipitation was beginning in the San Francisco Bay area (see inset in Fig. SB3). Data were collected along flight legs through and above the warm sector of the AR immediately offshore. A state-of-the art meteorology and trace gas payload collected in situ measurements used to examine the coastal barrier jet that is important to the position and intensity of the precipitation onshore during the landfalling AR event.

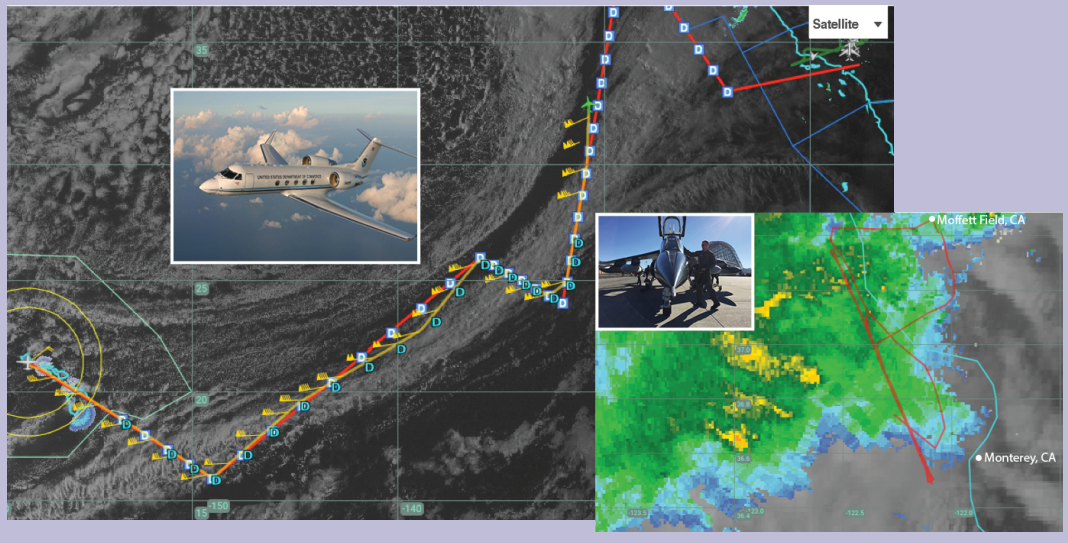


**FIG. SB3. G-IV planned (red) and executed (yellow) tracks for the 10 Mar 2016 flight between Honolulu and Ontario, CA. Background imagery is from GOES-West visible at 0215 UTC 11 Mar 2016. (inset) Alpha Jet flight tracks that were completed off the coast west of San Jose and Monterey Bay, CA, overlaid on Next Generation Weather Radar (NEXRAD) base reflectivity at 0000 UTC 11 Mar 2016 just after the jet landed back at Moffett Field and a couple hours prior to the GOES-West image in the larger graphic. Both images were adapted from the NASA MTS provided courtesy of Aaron Duley (NASA Ames).**

different spatial and temporal sampling, requiring adjustments to allow for direct comparison (see supplement for details of this collocation method). Comparisons of the dropsonde data with satellite soundings (Fig. 10b) indicate that at most latitudes, the dropsonde data are drier from approximately 850 to 700 hPa, with the relative dryness extending through a deeper layer just north of the equator, close to the latitude where convection was typically most intense (cf. Fig. 6). Conversely, the dropsonde data show relatively moister values than the NUCAPS soundings near 850 hPa at most latitudes northward of approximately 3°N, with drier values below. Comparisons between the dropsonde data and GFS analyses (Fig. 10c) show a qualitatively similar pattern but with more uniformly negative differences extending over a deeper layer near the latitude of maximum convection. In the boundary layer, where satellite-based radiance measurements contain less information as a result of the opacity of the atmosphere, satellite soundings have poorer vertical resolution than the dropsondes. Also, infrared radiances can be detrimentally impacted by clouds. Similar limitations also impact the GFS analysis and forecasts. Both issues may explain the differences observed in the top-right and bottom-left panels. In all comparisons, $\theta_e$ and $q$ differences are strongly

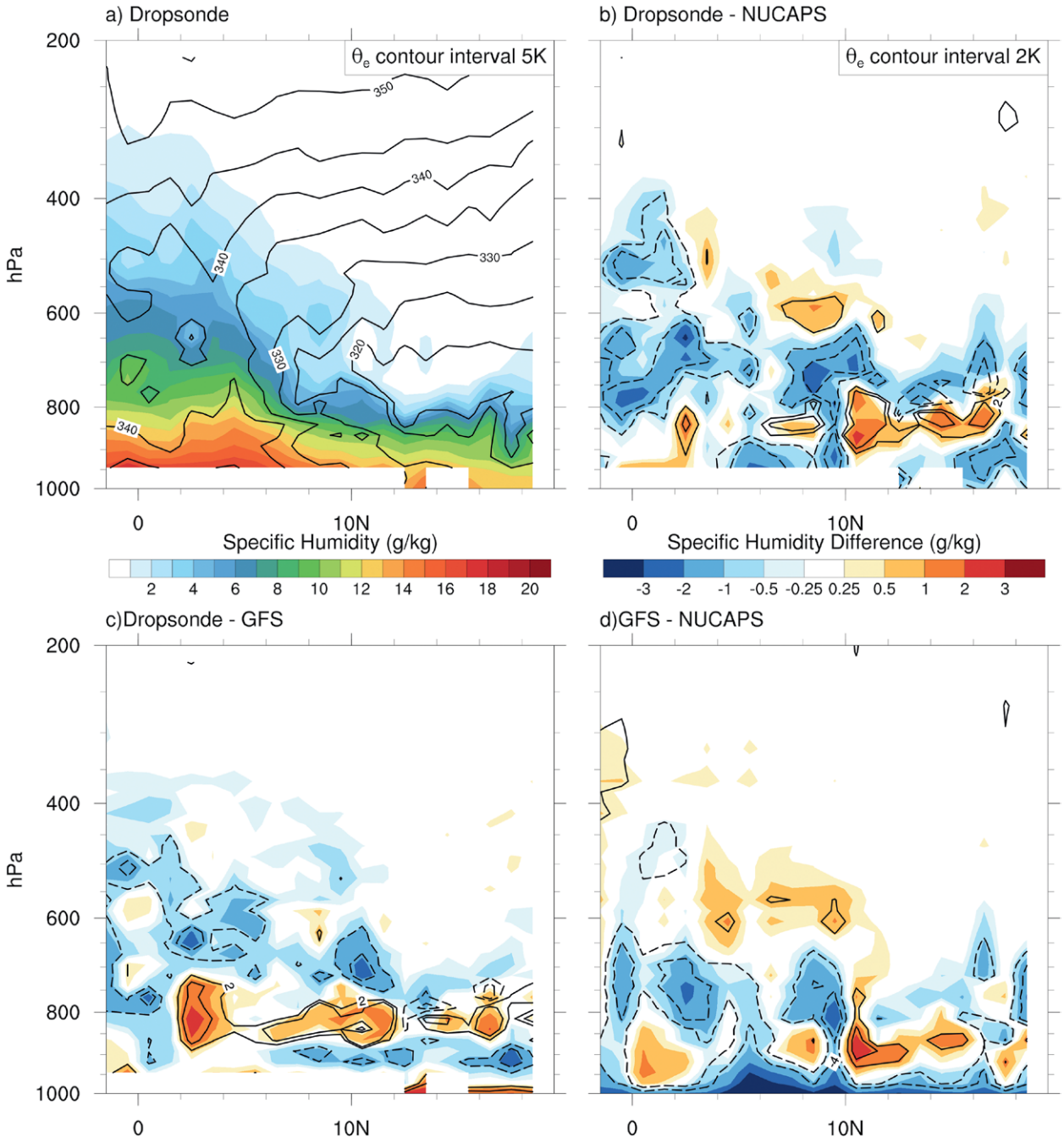


**Fig. 10. Comparisons of vertical profiles of ENRR G-IV dropsonde data, NOAA NUCAPS satellite retrievals, and GFS model analyses for $q$ and $\theta_e$. Latitude–height plots are zonal averages from 162° to 150°W. (a) Dropsonde sounding values are averaged over all flight days. Shown are specific humidity (shading) and equivalent potential temperature (contours). Contour intervals are 2 K, with negative values dashed (zero contour not shown). (b) Mean differences between dropsonde and NUCAPS soundings at the dropsonde location. (c) Mean differences between dropsonde and GFS soundings at the dropsonde location. (d) Mean differences between GFS and NUCAPS soundings at the NUCAPS location.**

positively correlated, suggesting that differences in equivalent potential temperature vertical structures may be primarily explained by moisture differences. The comparison of GFS with NUCAPS (Fig. 10d) also shows notable differences. Addressing many of these issues will require more extensive diagnostic analyses, including consideration of sampling issues, the collocation strategy, and the effective vertical resolution of both NUCAPS soundings and GFS fields in relation to the higher dropsonde resolution.

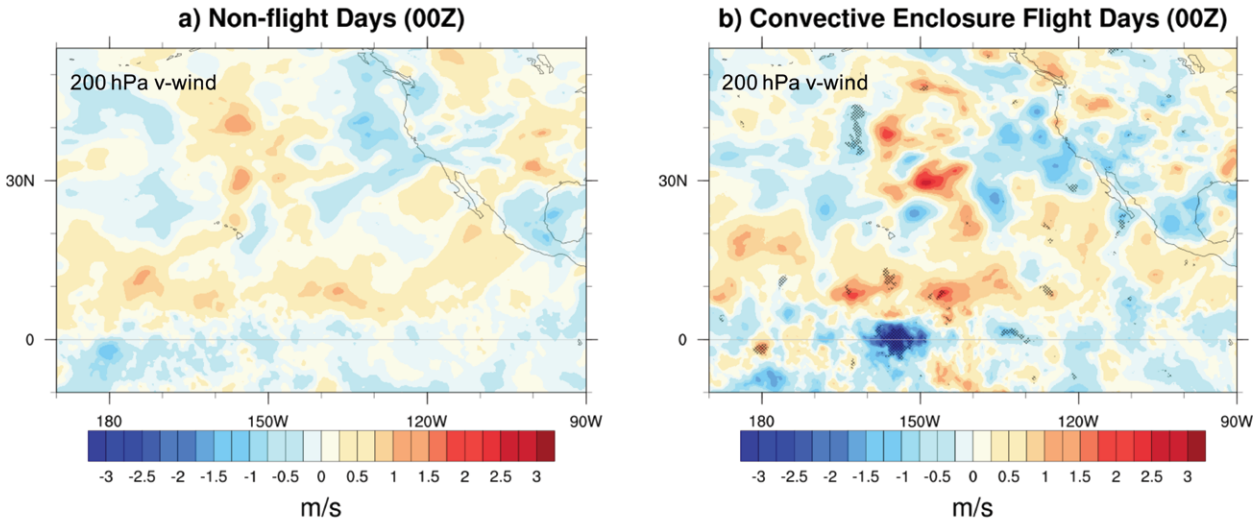


**Fig. 11. Meridional wind (m $s^{-1}$) analysis increments at 200 hPa and 0000 UTC in the NOAA GFS model averaged over all (a) nonflight days between 21 Jan and 31 Mar and (b) convective enclosure flight days (Table 6). Convective enclosure flights crossed south of the region of maximum convection, typically located between 2° and 6°N. Timing of the flights was such that dropsonde observations were taken after the 1800 UTC analysis period on the flight day; thus, they did not affect that analysis or the 6-h forecast (first guess) fields for 0000 UTC but were available for the 0000 UTC analysis. Color bar indicates systematic tendency toward stronger northerly winds in the analysis compared to the forecast (blue) and stronger southerly flow in the analysis than the forecast (red). Stippling in (b) shows the 2.5% significance level for differences in the distribution between the nonflight and convective enclosure flight days as determined from a Kolmogorov–Smirnov test.**

*Impact of ENRR observations of GFS analyses.* A fundamental practical question is, what impact did the field campaign observations have on model-based analyses, especially in operational global weather models during the field campaign? Here we present an early result for the NOAA GFS operational model analyses. In this example, *analysis increments*, calculated as differences between analyzed and first-guess 6-h forecast fields, are studied. These differences provide a measure of the impact of observations on model-based analyses.

Analysis increments were calculated for several variables for the 0000 UTC analyses during the field campaign. Figure 11a shows the composite mean analysis increment for 0000 UTC analyses calculated over *all G-IV nonflight days* of 200-hPa meridional winds $v_{200}$ during the ENRR field campaign (21 January–31 March). For the nonflight days, the mean analysis increment shows increased northward flow to the north of the latitude of maximum convection and increased southward flow to the south. This pattern suggests that the GFS model 6-h forecast systematically underestimates the strength of the 200-hPa meridional divergence out of the ITCZ (shifted southward during El Niño), with observations (not including the G-IV) assimilated during the analysis producing an increment that strengthens the outflow in the 0000 UTC analysis.

To look for impacts of G-IV dropsonde observations, increments were also calculated for the 10 *G-IV convective enclosure flight days* (see Fig. 1; Table 6), during which flights penetrated deep into the tropics to the south of the maximum convection (cf. Fig. 1). The $v_{200}$ analysis increments for the flight days (Fig. 11b) resemble the nonflight days in showing a north–south dipole of strengthened outflow straddling the maximum convection, but in the flight days the increased outflow is substantially larger. The results for both nonflight and flight days suggest that during the campaign period, the upper-level meridional outflow from the convective region is systematically too weak in the GFS forecast compared with observations. The additional G-IV data increase this upper-level meridional flow, suggesting that this difference may not be fully corrected by routine observations from the global observing system. While these early results are suggestive, they are not conclusive. They have motivated more comprehensive experiments to examine the impacts of the ENRR field campaign data on GFS analyses, with possible implications for future observing systems.

*Impact of ENRR observations on NASA GEOS model forecasts during the field campaign.* A second fundamental question is, what impact did the field campaign observations have on forecasts? Rigorous

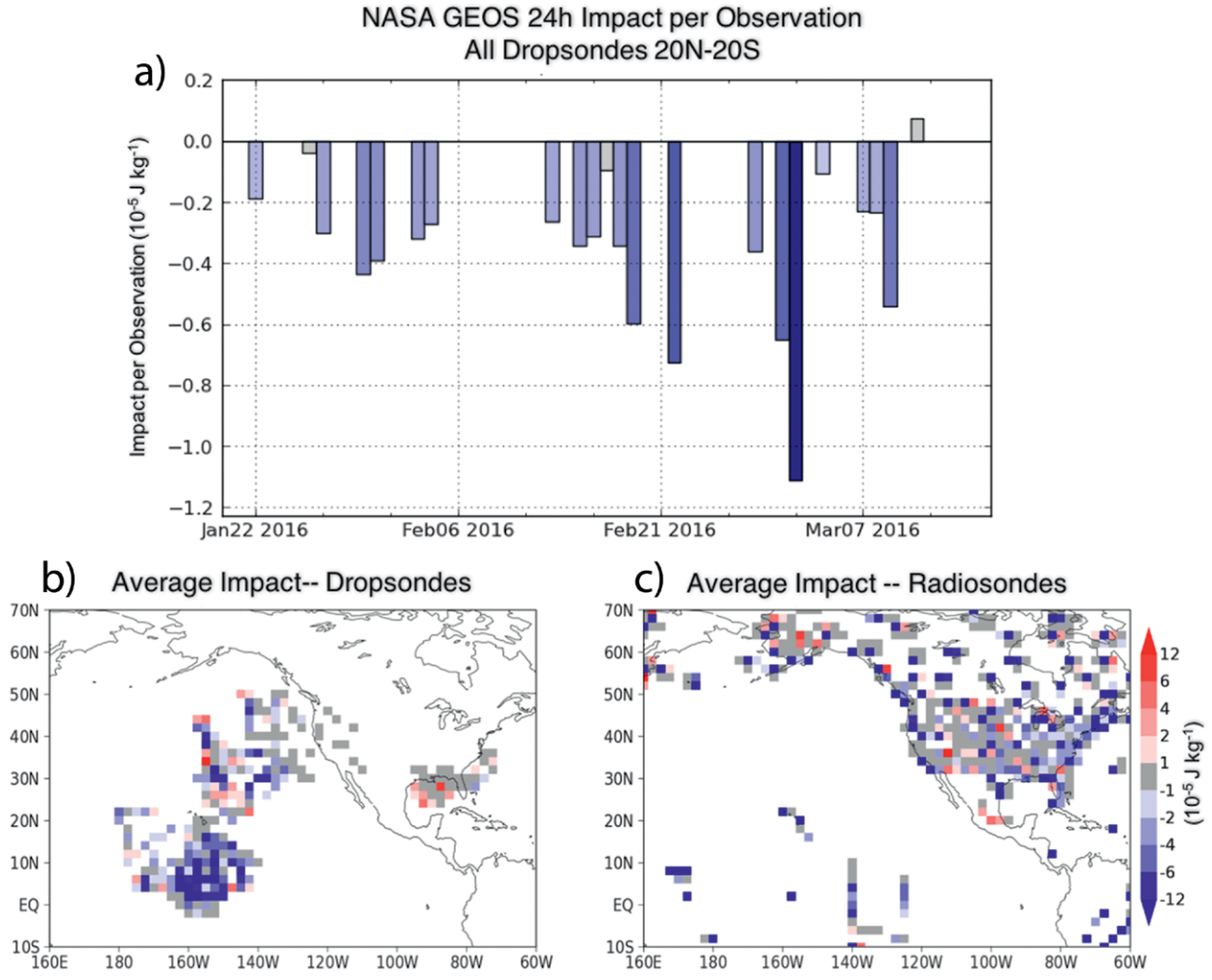


**Fig. 12. (a) Net impact of dropsonde observations deployed between 20°N and 20°S on NASA GEOS model 24-h forecasts of global moist energy for forecasts beginning at 0000 UTC, shown for ENRR G-IV flight days over the period 20 Jan–16 Mar 2016. Time-average maps over the same period of the impact of observations at different locations on NASA GEOS 24-h model forecasts of global moist energy as a result of (b) dropsondes and (c) radiosondes. Locations are displayed as 2° × 2° gridbox average values. Negative values (shaded blue) indicate observations inside a grid box reduced errors in this global forecast error metric, with positive values (shaded red) indicating increased errors. White areas are locations where no observations of the specified type were taken during the period; consequently, they contributed no observational impact on forecast skill for this metric. The units are $10^{-5}$ J kg$^{-1}$ in all panels.**

assessments of the impacts of ENRR field campaign observations on GFS forecasts, including over specific regions such as North America, will require reforecasting with data denial experiments. Important initial insights can be gained now, however, from results obtained from the NASA Goddard Earth Observing System (GEOS) Global Data Assimilation System (GDAS), which is also run routinely in real-time analysis/forecast mode, allowing an initial assessment of impacts of different observations on forecast quality.

ENRR field campaign observations were assimilated in real time into GEOS GDAS. Their impact on 24-h forecast errors, measured in terms of global moist energy (J kg$^{-1}$), was calculated using the adjoint of the GEOS data assimilation system (e.g., Gelaro et al. 2010). The measure combines errors in surface pressure and wind, temperature, and specific humidity from the surface to 1 hPa. Observation impacts were computed once daily for the 24-h forecast initialized at 0000 UTC as part of the GEOS operational suite. Results were made available in near–real time via the Global Modeling and Assimilation Office (GMAO)'s web page (https://gmao.gsfc.nasa.gov/forecasts/systems/fp/obs_impact/) and used for diagnostic and planning purposes during the campaign.

The time series in Fig. 12a shows the combined impact of dropsonde observations deployed between 20°N and 20°S for each case in which these data were assimilated during the ENRR field campaign period. Negative (positive) values indicate that the assimilated observations have improved (degraded) the forecast. Here the impacts are normalized by the number of dropsonde observations assimilated in each case. The results show that the ENRR dropsonde observations reduced the global 24-h forecast error measure in almost all cases. No other component of the tropical observing system contributed more to the overall reduction of this error measure on a per-observation basis during the campaign period (not shown).

Figures 12b and 12c show the time-averaged spatial distribution of observation impacts for dropsondes and radiosondes, respectively, over the eastern North Pacific–North American region during the campaign period. These results represent 2° × 2° gridded box-average values of the observation locations and their impact on the global forecast error measure. The ENRR dropsonde deployments over the eastern North Pacific are prominent in Fig. 12b, while radiosondes from the routine upper-air network over land provide most observations in Fig. 12c. Impacts of the ENRR radiosonde launches from the *RHB* (deployed along 125° and 140°W close to the equator) and from Kiritimati are also evident in Fig. 12c. Figure 12b shows that large forecast error reductions resulted from the deployment of ENRR dropsondes to the south and southwest of Hawaii, with smaller error reductions and more neutral and mixed impacts from the deployments to the northeast. Overall, the dropsonde impacts were clearly beneficial and comparable to those obtained from the routine radiosonde network. Radiosondes deployed from the *RHB* and Kiritimati also had a clear overall beneficial impact.

The scattered occurrence of nonbeneficial impacts evident in Figs. 12b and 12c is expected, owing to the statistical nature and other properties of the data assimilation system (e.g., Ehrendorfer 2007), and consistent with those reported for other data types and forecast systems (Gelaro et al. 2010; Lorenc and Marriott 2014; Majumdar 2016). At the same time, more coherent patterns of nonbeneficial impact, such as that seen for dropsondes (not associated with ENRR) over the northwestern Gulf of Mexico in Fig. 12b, may be indicative of deficiencies in either the quality or use of observations in those locations, which may warrant further investigation.

**SUMMARY.** El Niño forecasts in summer 2015 presented an exceptional scientific opportunity to advance understanding and predictions of a strong climate event while also supporting NOAA's services during the event. Seizing this opportunity, NOAA initiated a coordinated rapid response to El Niño.

As part of the ENRR, NOAA developed a field campaign to obtain intensive atmospheric observations from the tropical Pacific to the U.S. West Coast, with a primary focus on atmospheric conditions over the central tropical Pacific near the heart of El Niño. The initial atmospheric response in this region serves as a critical first link that connects El Niño to impacts over the United States and elsewhere. The campaign was conceived, planned, and executed in less than 6 months—much less time than normally required for a field campaign to a remote region. By conducting its operations during the event, the campaign achieved dual objectives of supporting real-time operational predictions and obtaining data for future research. Because of its rapidity, intensive atmospheric observations were obtained for the first time in the region of enhanced convection over the tropical Pacific during El Niño.

Given doubts about whether a major field campaign could even be mounted within the lead time provided by El Niño forecasts, perhaps the most significant finding is that a rapid response field campaign is possible now. While traditional field campaigns will continue to be of primary importance, rapid response campaigns provide new opportunities to obtain additional observations during rare or high-impact climate events that would otherwise be missed. The feasibility of developing a rapid scientific response to climate predictions also can strengthen research-services collaborations to accelerate research advances while simultaneously supporting operational services.

Learning from the present experience, future responses could be enhanced through preplanning response options and identifying coordination opportunities for specific phenomena or events. Beyond NOAA, such efforts should engage the broader scientific community, including academic, interagency, and international partners. Taking these steps would help bring to bear additional assets and ensure questions that were not addressed in this campaign will be next time.

Initial results presented here, while tentative, point to possible systematic model deficiencies and to impacts of the field campaign observations on global predictions and model-based analyses. Impacts on U.S. forecasts are now being investigated. Tropical precipitation variability during the strong El Niño proved particularly challenging for models to predict, affecting flight planning and operations, and potentially conditions outside the tropics as well. An important and related question is why heavy rains anticipated for Southern California and the southwestern United

States failed to materialize as in previous strong events (Zhang et al. 2018). These and other outstanding issues are now being investigated.

While many results from the ENRR remain to be determined, it is clear now that a rapid response field campaign to El Niño is feasible and can provide valuable contributions to advancing both science and services. Active collaborations between research and services during high-impact climate events like the 2015/16 El Niño provide rich opportunities to strengthen capabilities, simultaneously supporting services during the event while also accelerating research to address major science challenges. As demonstrated in the NOAA ENRR, both research and services benefit from strong and proactive coordination during high-impact climate events.

**ACKNOWLEDGMENTS.** We greatly appreciate the contributions in record time from many people within NOAA (OAR, NWS, OMAO, NESDIS), including those in senior leadership positions, intra-agency El Niño Rapid Response Coordination Team members, and staff providing vital logistics and budget support. We thank the OMAO Aircraft Operations Center, especially Project Manager Jack Parrish and the NOAA G-IV pilots and crew, for their dedication and support throughout the campaign, which included the first crossing by this aircraft into the Southern Hemisphere, as well as the National Data Buoy Center and OMAO Marine Operations Center, including Operations Officer Adrienne Hopper and the entire *RHB* crew for graciously hosting and supporting ENRR participants on the TAO buoy survey. We thank the NOAA UAS Program, including Program Director Robbie Hood and the SHOUT instrument and science teams, the joint efforts of Frank Cutler, Cdr. Jonathan Neuhaus, and the NASA Armstrong Flight Research Center and NOAA AOC aircraft teams for their coordination with ENRR. Many contributions were essential to enabling the ENRR to conduct radiosonde balloon launches from Kiritimati, including Arthur Paterson, OAR International Affairs; Jennifer Lewis, NWS International Activities Office; the Honolulu-based NOAA staff; Mark Mineo, U.S. State Department; the Kiribati Meteorological Services (Ueneta Toorua); and the proprietors of the Captain Cook Hotel. The Decca site is operated by the Kiritimati Island Water Project, which is funded by the European Union (EU) and implemented by the Secretariat of the Pacific Community (SPC). Data from the Decca site and from the official Kiribati Meteorological Service were provided by Tony Falkland, Island Hydrology Services, Canberra, Australia. Thanks to Deon Terblanche and Paolo Ruti of the World Meteorological Organization and Philippe Bougeault of Météo-France for their help expediting the required invitations, clearances, and visas for crew into French Polynesia should diversions to that area be needed during the campaign. Others supporting ENRR included Laura Iraci, NASA Ames Research Center, for coordinating the Alpha Jet Atmospheric Experiment (AJAX) with the final G-IV flight; Marty Ralph, Scripps Institution of Oceanography, for coordinating the extratropical atmospheric river C-130s flights; Aaron Duley, NASA Ames Research Center, for providing support in the use of MTS; Ryan Maue, Weather Bell Analytics, for creating special grids over the ENRR campaign domain and for providing access to model graphics; and Natalia Donoho, NESDIS, for tailoring GOES imagery for the ENRR campaign. We also thank Dr. Arun Kumar and two anonymous reviewers for their thoughtful and constructive comments and suggestions toward improving this article. The scientific results and conclusions, as well as any views or opinions expressed herein, are those of the authors and do not necessarily reflect the views of NOAA or the Department of Commerce.

## REFERENCES

Barsugli, J. J., and P. D. Sardeshmukh, 2002: Global atmospheric sensitivity to tropical SST anomalies throughout the Indo-Pacific basin. *J. Climate*, **15**, 3427–3442, https://doi.org/10.1175/1520-0442(2002)015<3427:GASTTS>2.0.CO;2.

Bauer, P., A. Thorpe, and G. Brunet, 2015: The quiet revolution of numerical weather prediction. *Nature*, **525**, 47–55, https://doi.org/10.1038/nature14956.

Bjerknes, J., 1966: A possible response of the atmospheric Hadley circulation to equatorial anomalies of ocean temperature. *Tellus*, **18**, 820–829, https://doi.org/10.3402/tellusa.v18i4.9712.

——, 1969: Atmospheric teleconnections from the equatorial Pacific. *Mon. Wea. Rev.*, **97**, 163–172, https://doi.org/10.1175/1520-0493(1969)097<0163:ATFTEP>2.3.CO;2.

Bove, M., D. Zierden, and J. O'Brien, 1998: Are Gulf landfalling hurricanes getting stronger? *Bull. Amer. Meteor. Soc.*, **79**, 1327–1328, https://doi.org/10.1175/1520-0477(1998)079<1327:AGLHGS>2.0.CO;2.

Capotondi, A., and Coauthors, 2015: Understanding ENSO diversity. *Bull. Amer. Meteor. Soc.*, **96**, 921–938, https://doi.org/10.1175/BAMS-D-13-00117.1.

Chagnon, S. A., Ed., 2000: *El Niño, 1997–1998: The Climate Event of the Century*. Oxford University Press, 232 pp.

Cifelli, R., V. Chandrasekar, H. Chen, and L. E. Johnson, 2018: High resolution radar quantitative precipitation estimation in the San Francisco Bay area: Rainfall monitoring for the urban environment. *J. Meteor. Soc. Japan*, https://doi.org/10.2151/jmsj.2018-016, in press.

Cox, C., and L. Hartten, 2017: El Niño Rapid Response (ENRR) Field Campaign: Surface flux data from

the NOAA Ship Ronald H. Brown, 2016-02 to 2016-03 (NCEI accession 0167875), version 1.1. NOAA/National Centers for Environmental Information, accessed 20 December 2018, https://doi.org/10.7289/V58050VP.

——, D. Wolfe, L. Hartten, and P. Johnston, 2017a: El Niño Rapid Response (ENRR) field campaign: Radiosonde data (level 2) from the NOAA ship Ronald H. Brown, February–March 2016 (NCEI accession 0161527), version 1.1. NOAA/National Centers for Environmental Information, accessed 21 June 2017, https://doi.org/10.7289/V5X63K15.

——, ——, ——, and ——, 2017b: El Niño Rapid Response (ENRR) field campaign: Surface meteorological and ship data from the NOAA ship Ronald H. Brown, February-March 2016 (NCEI accession 0161528), version 1.1. NOAA/National Centers for Environmental Information, accessed 21 June 2017, https://doi.org/10.7289/V5SF2T80.

CPC/IRI, 2015: IRI ENSO forecast: 2015 July quick look. Accessed 20 March 2018, https://iri.columbia.edu/our-expertise/climate/forecasts/enso/2015-July-quick-look/.

Deser, C., I. R. Simpson, K. A. McKinnon, and A. S. Phillips, 2017: The Northern Hemisphere extratropical atmospheric circulation response to ENSO: How well do we know it and how do we evaluate models accordingly? *J. Climate*, **30**, 5059–5082, https://doi.org/10.1175/JCLI-D-16-0844.1.

Earth Observing Laboratory, 2016: SHOUT-ENRR Global Hawk QC dropsonde data, version 1.0. UCAR/NCAR, accessed 20 December 2016, https://doi.org/10.5065/D66W9848.

——, 2017: ASPEN. NCAR/UCAR, accessed 26 June 2017, www.eol.ucar.edu/software/aspen.

Ehrendorfer, M., 2007: A review of issues in ensemble-based Kalman filtering. *Meteor. Z.*, **16**, 795–818, https://doi.org/10.1127/0941-2948/2007/0256.

Gage, K. S., B. B. Balsley, W. L. Ecklund, D. A. Carter, and J. R. McAfee, 1991: Wind profiler-related research in the tropical Pacific. *J. Geophys. Res.*, **96**, 3209–3220, https://doi.org/10.1029/90JD01829.

Gambacorta, A., 2013: The NOAA Unique CrIS/ATMS Processing System (NUCAPS): Algorithm theoretical basis documentation. NOAA Rep., 73 pp., www.ospo.noaa.gov/Products/atmosphere/soundings/nucaps/docs/NUCAPS_ATBD_20130821.pdf.

——, C. Barnet, and M. Goldberg, 2015: Status of the NOAA Unique CrIS/ATMS Processing System (NUCAPS): Algorithm development and lessons learned from recent field campaigns. *Proc. 20th Int. TOVS Study Conf.*, Lake Geneva, WI, International ATOVS Working Group, 4.01, https://cimss.ssec.wisc.edu/itwg/itsc/itsc20/program/PDFs/29Oct/session4a/4_01_gambacorta.pdf.

Gelaro, R., R. H. Langland, S. Pellerin, and R. Todling, 2010: The THORPEX observation impact intercomparison experiment. *Mon. Wea. Rev.*, **138**, 4009–4025, https://doi.org/10.1175/2010MWR3393.1.

Glantz, M., 2000: *Currents of Change—Impacts of El Niño and La Niña on Climate and Society*. 2nd ed. Cambridge University Press, 268 pp.

Gray, W. M., 1984: Atlantic seasonal hurricane frequency. Part I: El Niño and 30 mb quasi-biennial oscillation influences. *Mon. Wea. Rev.*, **112**, 1649–1668, https://doi.org/10.1175/1520-0493(1984)112<1649:ASHFPI>2.0.CO;2.

Halpert, M. S., and C. F. Ropelewski, 1992: Surface temperature patterns associated with the Southern Oscillation. *J. Climate*, **5**, 577–593, https://doi.org/10.1175/1520-0442(1992)005<0577:STPAWT>2.0.CO;2.

Hamill, P., L. T. Iraci, E. L. Yates, W. Gore, T. P. Bui, T. Tanaka, and M. Loewenstein, 2016: A new instrumented airborne platform for atmospheric research. *Bull. Amer. Meteor. Soc.*, **97**, 397–404, https://doi.org/10.1175/BAMS-D-14-00241.1.

Hartten, L. M., C. J. Cox, P. E. Johnston, D. E. Wolfe, S. Abbott, and H. A. McColl, 2017a: Central-Pacific surface meteorology from the 2016 El Niño Rapid Response (ENRR) field campaign. *Earth Syst. Sci. Data Discuss.*, https://doi.org/10.5194/essd-2017-126.

——, P. Johnston, C. Cox, and D. Wolfe, 2017b: El Niño Rapid Response (ENRR) field campaign: Radiosonde data (level 2) from Kiritimati Island, January-March 2016 (NCEI accession 0161525), version 1.1. NOAA/National Centers for Environmental Information, accessed 21 June 2017, https://doi.org/10.7289/V55Q4T5K.

——, ——, ——, and ——, 2017c: El Niño Rapid Response (ENRR) field campaign: Surface meteorological data from Kiritimati Island, January-March 2016 (NCEI accession 0161526), version 1.1. NOAA/National Centers for Environmental Information, accessed 21 June 2017, https://doi.org/10.7289/V51Z42H4.

——, C. J. Cox, P. E. Johnston, D. E. Wolfe, S. Abbott, H. A. McColl, X.-W. Quan, and M. G. Winterkorn, 2018: Ship- and island-based soundings from the 2016 El Niño Rapid Response (ENRR) field campaign. *Earth Syst. Sci. Data Discuss.*, https://doi.org/10.5194/essd-2018-7.

Hoell, A., M. Hoerling, J. Eischeid, K. Wolter, R. Dole, J. Perlwitz, T. Xu, and L. Cheng, 2016: Does El Niño intensity matter for California precipitation? *Geophys. Res. Lett.*, **43**, 819–825, https://doi.org/10.1002/2015GL067102.

Hoerling, M. P., and A. Kumar, 2002: Atmospheric response patterns associated with tropical forcing. *J. Climate*, **15**, 2184–2203, https://doi.org/10.1175/1520-0442(2002)015<2184:ARPAWT>2.0.CO;2.

Horel, J. D., and J. M. Wallace, 1981: Planetary-scale atmospheric phenomena associated with the Southern Oscillation. *Mon. Wea. Rev.*, **109**, 813–829, https://doi.org/10.1175/1520-0493(1981)109<0813:PSAPAW>2.0.CO;2.

Kiladis, G. N., and H. F. Diaz, 1989: Global climatic anomalies associated with extremes in the Southern Oscillation. *J. Climate*, **2**, 1069–1090, https://doi.org/10.1175/1520-0442(1989)002<1069:GCAAWE>2.0.CO;2.

——, M. C. Wheeler, P. T. Haertel, K. H. Straub, and P. E. Roundy, 2009: Convectively coupled equatorial waves. *Rev. Geophys.*, **47**, RG2003, https://doi.org/10.1029/2008RG000266.

Kumar, A., and M. P. Hoerling, 1997: Interpretation and implications of observed inter-El Niño variability. *J. Climate*, **10**, 83–91, https://doi.org/10.1175/1520-0442(1997)010<0083:IAIOTO>2.0.CO;2.

——, and ——, 1998: Annual cycle of Pacific North American seasonal predictability associated with different phases of ENSO. *J. Climate*, **11**, 3295–3308, https://doi.org/10.1175/1520-0442(1998)011<3295:ACOPNA>2.0.CO;2.

——, and M. Chen, 2017: What is the variability in US West Coast winter precipitation during strong El Niño events? *Climate Dyn.*, **49**, 2789, https://doi.org/10.1007/s00382-016-3485-9.

Langland, R. H., and Coauthors, 1999: The North Pacific Experiment (NORPEX-98): Targeted observations for improved North American weather forecasts. *Bull. Amer. Meteor. Soc.*, **80**, 1363–1384, https://doi.org/10.1175/1520-0477(1999)080<1363:TNPENT>2.0.CO;2.

Leetmaa, A., 1999: The first El Niño observed and forecasted from start to finish. *Bull. Amer. Meteor. Soc.*, **80**, 111–112.

L'Heureux, M. L., and Coauthors, 2017: Observing and predicting the 2015/16 El Niño. *Bull. Amer. Meteor. Soc.*, **98**, 1363–1382, https://doi.org/10.1175/BAMS-D-16-0009.1.

Lorenc, A. C., and R. T. Marriott, 2014: Forecast sensitivity to observations in the Met Office global numerical weather prediction system. *Quart. J. Roy. Meteor. Soc.*, **140**, 209–224, https://doi.org/10.1002/qj.2122.

Majumdar, S. J., 2016: A review of targeted observations. *Bull. Amer. Meteor. Soc.*, **97**, 2287–2303, https://doi.org/10.1175/BAMS-D-14-00259.1.

McPhaden, M. J., 2015: Playing hide and seek with El Niño. *Nat. Climate Change*, **5**, 791–795, https://doi.org/10.1038/nclimate2775.

——, S. E. Zebiak, and M. H. Glantz, 2006: ENSO as an integrating concept in Earth science. *Science*, **314**, 1740–1745, https://doi.org/10.1126/science.1132588.

——, A. Timmermann, M. J. Widlansky, M. A. Balmaseda, and T. N. Stockdale, 2015: The curious case of the El Niño that never happened: A perspective from 40 years of progress in climate research and forecasting. *Bull. Amer. Meteor. Soc.*, **96**, 1647–1665, https://doi.org/10.1175/BAMS-D-14-00089.1.

Moncrieff, M. W., D. E. Waliser, M. J. Miller, M. A. Shapiro, G. R. Asrar, and J. Caughey, 2012: Multiscale convective organization and the YOTC virtual global field campaign. *Bull. Amer. Meteor. Soc.*, **93**, 1171–1187, https://doi.org/10.1175/BAMS-D-11-00233.1.

Nalli, N. R., and Coauthors, 2013: Validation of satellite sounder environmental data records: Application to the Cross-Track Infrared Microwave Sounder Suite. *J. Geophys. Res. Atmos.*, **118**, 13 628–13 643, https://doi.org/10.1002/2013JD020436.

——, and Coauthors, 2018: Validation of atmospheric profile retrievals from the SNPP NOAA-Unique Combine Atmospheric Processing System. Part 1: Temperature and moisture. *IEEE Trans. Geosci. Remote Sens.*, **56**, 180–190, https://doi.org/10.1109/TGRS.2017.2744558.

Neiman, P. J., F. M. Ralph, A. B. White, D. E. Kingsmill, and P. O. G. Persson, 2002: The statistical relations between upslope flow and rainfall in California's coastal mountains: Observations during CALJET. *Mon. Wea. Rev.*, **130**, 1468–1492, https://doi.org/10.1175/1520-0493(2002)130<1468:TSRBUF>2.0.CO;2.

Newman, M., P. D. Sardeshmukh, and C. Penland, 2009: How important is air–sea coupling in ENSO and MJO evolution? *J. Climate*, **22**, 2958–2977, https://doi.org/10.1175/2008JCLI2659.1.

——, A. Wittenberg, L. Chang, G. P. Compo, and C. A. Smith, 2018: The extreme 2015/16 El Niño, in the context of historical climate variability and change. *Bull. Amer. Meteor. Soc.*, **99**, (Suppl.), https://doi.org/10.1175/BAMS-D-17-0116.1.

Quinn, W. H., 1974: Outlook for El Niño-like conditions in 1975. *NORPAX Highlights*, **2** (6), 2–3.

Ralph, F. M., P. J. Neiman, D. E. Kingsmill, P. O. G. Persson, A. B. White, E. T. Strem, E. D. Andrews, and R. C. Antweiler, 2003: The impact of a prominent rain shadow on flooding in California's Santa Cruz mountains: A CALJET case study and sensitivity to the ENSO cycle. *J. Hydrometeor.*, **4**, 1243–1264,

https://doi.org/10.1175/1525-7541(2003)004<1243:TIOAPR>2.0.CO;2.

——, and Coauthors, 2016: CalWater field studies designed to quantify the roles of atmospheric rivers and aerosols in modulating U.S. West Coast precipitation in a changing climate. *Bull. Amer. Meteor. Soc.*, **97**, 1209–1228, https://doi.org/10.1175/BAMS-D-14-00043.1.

Ropelewski, C. F., and M. S. Halpert, 1987: Global and regional scale precipitation patterns associated with the El Niño/Southern Oscillation. *Mon. Wea. Rev.*, **115**, 1606–1626, https://doi.org/10.1175/1520-0493(1987)115<1606:GARSPP>2.0.CO;2.

Scaife, A. A., and Coauthors, 2014: Skillful long-range prediction of European and North American winters. *Geophys. Res. Lett.*, **41**, 2514–2519, https://doi.org/10.1002/2014GL059637.

Schiermeier, Q., 2015: Hunting the Godzilla El Niño. *Nature*, **526**, 490–491, https://doi.org/10.1038/526490a.

Schonher, T., and S. E. Nicholson, 1989: The relationship between California rainfall and ENSO events. *J. Climate*, **2**, 1258–1269, https://doi.org/10.1175/1520-0442(1989)002<1258:TRBCRA>2.0.CO;2.

Shapiro, M. A., H. Wernli, N. A. Bond, and R. Langland, 2001: The influence of the 1997-99 El Niño Southern Oscillation on extratropical baroclinic life cycles over the eastern North Pacific. *Quart. J. Roy. Meteor. Soc.*, **127**, 331–342, https://doi.org/10.1002/qj.49712757205.

Stewart, S. R., 2016: National Hurricane Center annual summary: 2015 Atlantic hurricane season, 10 February 2016. NOAA/NWS/National Hurricane Center Rep., 16 pp., www.nhc.noaa.gov/data/tcr/summary_atlc_2015.pdf.

Trenberth, K. E., G. W. Branstator, D. Karoly, A. Kumar, N.-C. Lau, and C. Ropelewski, 1998: Progress during TOGA in understanding and modeling global teleconnections associated with tropical sea surface temperatures. *J. Geophys. Res.*, **103**, 14 291–14 324, https://doi.org/10.1029/97JC01444.

White, A. B., P. J. Nieman, F. M. Ralph, D. E. Kingsmill, and P. O. G. Persson, 2003: Coastal orographic rainfall processes observed by radar during the California Land-Falling Jets Experiment. *J. Hydrometeor.*, **4**, 264–282, https://doi.org/10.1175/1525-7541(2003)4<264:CORPOB>2.0.CO;2.

Wick, G., J. Dunion, and J. Walker, 2018: Sensing hazards with operational unmanned technology: Impact study of Global Hawk unmanned aircraft system observations for hurricane forecasting, final report. NOAA Tech Memo. OAR-UAS-002, 93 pp., ftp://ftp1.esrl.noaa.gov/et6/sat/shout/data_impact/TM_SHOUT_Impact_Assessment_FINAL.pdf.

Wolfe, D., K. Cobb, C. Smith, 2017: Temperature, salinity and other parameters from CTDs from NOAA ship Ronald H. Brown during the 2016 El Niño Rapid Response (ENRR) campaign (NCEI Accession 0162434), version 1.1. NOAA/National Centers for Environmental Information, accessed 21 June 2017, https://data.nodc.noaa.gov/cgi-bin/iso?id=gov.noaa.nodc:0162434.

Zhang, T., and Coauthors, 2018: Predictability and prediction of the Southern California rains during strong El Niño events: A focus on the failed 2016 winter rains. *J. Climate*, **31**, 555–574, https://doi.org/10.1175/JCLI-D-17-0396.1.

# Radar and Atmospheric Science: A Collection of Essays in Honor of David Atlas

Edited by Roger M. Wakimoto and Ramesh Srivastava

This monograph pays tribute to one of the leading scientists in meteorology, Dr. David Atlas. In addition to profiling the life and work of the acknowledged "Father of Radar Meteorology," this collection highlights many of the unique contributions he made to the understanding of the forcing and organization of convective systems, observation and modeling of atmospheric turbulence and waves, and cloud microphysical properties, among many other topics. It is hoped that this text will inspire the next generation of radar meteorologists, provide an excellent resource for scientists and educators, and serve as a historical record of the gathering of scholarly contributions honoring one of the most important meteorologists of our time.

**Radar and Atmospheric Science: A Collection of Essays in Honor of David Atlas**

Aug 2003. Meteorological Monograph Series, Vol. 30, No. 52; 270 pp, hardbound; ISBN 1-878220-57-8; AMS code MM52.

**Price** $80.00 member

**To place an order** point your Web browser to www.ametsoc.org/amsbookstore

AMS BOOKS

RESEARCH ◆ APPLICATIONS ◆ HISTORY